



Origin and evolution of post-collisional magmatism: Coeval Neoproterozoic calc-alkaline and alkaline suites of the Sinai Peninsula

M. Eyal^a, B. Litvinovsky^{a,*}, B.M. Jahn^b, A. Zanzvilevich^a, Y. Katzir^a

^a Dept. of Geological and Environmental Sciences, Ben Gurion University of the Negev, Beer Sheva 84105, Israel

^b Institute of Earth Sciences, Academia Sinica, Taipei 11529, Taiwan

ARTICLE INFO

Article history:

Received 9 June 2009

Received in revised form 7 September 2009

Accepted 9 September 2009

Editor: R.L. Rudnick

Keywords:

Calc-alkaline

Peralkaline granite

Post-collisional magmatism

Radiogenic isotopes

Arabian–Nubian Shield

Sinai Peninsula

ABSTRACT

Two Late Neoproterozoic post-collisional igneous suites, calc-alkaline (CA) and alkaline–peralkaline (Alk), widely occur in the northernmost part of the Arabian–Nubian Shield. In Sinai (Egypt) and southern Israel they occupy up to 80% of the exposed basement. Recently published U–Pb zircon geochronology indicates a prolonged and partially overlapping CA and Alk magmatism at 635–590 Ma and 608–580 Ma, respectively. Nevertheless in each particular locality CA granitoids always preceded Alk plutons. CA and Alk igneous rocks have distinct chemical compositions, but felsic and mafic rocks in general and granitoids from the two suites in particular cannot be distinguished by their Nd, Sr and O isotope ratios. Both suites are characterized by positive $\epsilon_{\text{Nd}(T)}$ values, from +1.5 to +6.0 (150 samples, 28 of them are new analyses), but predominance of juvenile crust in the region prevents unambiguous petrogenetic interpretation of the isotope data. Comparison of geochemical traits of felsic and mafic rocks in each suite suggests a significant contribution of mantle-derived components to the silicic magmas. Model calculation shows that the alkaline granite magma could have been produced by partial (~20%) melting of rocks corresponding to K-rich basalts. Material balance further suggests that granodiorite and quartz monzonite magmas of the CA suite could form by mixing of the granite and gabbro end-members at proportions of 85/15. In the Alk suite, alkali feldspar and peralkaline granites have evolved mainly by fractional crystallization of feldspars and a small amount of mafic minerals from a parental syenogranite melt. Thus the protracted, 20 m.y. long, contemporaneous CA and Alk magmatism in the northern ANS requires concurrent tapping of two distinct mantle sources. Coeval emplacement of CA and Alk intrusive suites was described in a number of regions throughout the world.

© 2009 Elsevier B.V. All rights reserved.

1. Introduction

Post-collisional periods are characterized by voluminous, mostly granitoid magmatism (Liégeois, 1998). Whereas collision, the period of maximum convergence, is not favorable for magma ascent, post-collisional settings may involve large-scale tectonic movements with extensional component impelling magmatism. Since post-collisional settings are highly complicated and may include crustal-scale horizontal shear zones, transtensional domains and rifts, magmas of variable sources and types may be generated. Among these, two types of post-collisional magmas are dominant: high-K calc-alkaline and alkaline–peralkaline granitoids (Liégeois, 1998; Bonin, 2004).

Widespread Late Neoproterozoic magmatism terminated a major orogenic event recorded throughout Gondwana (i.e., Pan-African, Brasiliano, Cadomian) and formed several post-collisional igneous

provinces in Africa, South America and Europe. The Arabian–Nubian Shield (ANS; Fig. 1, inset), evolved as the northern segment of the East African orogen (900–530 Ma), is one of the best sites to determine the sources of post-collisional magmatism. The crust of the ANS is essentially juvenile formed solely by protracted accretion of island arc terranes (Bentor, 1985; Stern, 1994; Stein and Goldstein, 1996; Stern, 2002; Meert, 2003; Jarrar et al., 2003; Johnson, 2003; Johnson and Woldehaimanot, 2003; Stoesser and Frost, 2006). This allows avoiding the complications set by the contribution of pre-Neoproterozoic crust that occurs, for example, in other parts of the Pan-African orogen (e.g. the Saharan Metacraton, Küster et al., 2008). Thus the sources available for extraction of magma at the post-collisional period in the ANS are rather constrained in age and geochemical affinity.

Island arc accretion is thought to have ended in the ANS by ~700 Ma and followed by continental collision at 640–650 Ma (Stern, 1994 and references therein). The Late Neoproterozoic post-collisional stage of tectonomagmatic evolution of the ANS commenced at ~640 Ma. Transition from convergence to extension occurred at ~600 Ma (Stern, 1994; Garfunkel, 1999; Genna et al., 2002; Jarrar et al., 2003) and was finally followed with a stable craton and platform setting (Garfunkel, 1999). The evolution of the ANS

* Corresponding author. Tel.: +972 8 6477522 (work), +972 8 991 1307 (home); fax: +972 8 64 72 997.

E-mail addresses: moey@bgu.ac.il (M. Eyal), borisl@bgu.ac.il, borislit@mishmarhanegev.org.il (B. Litvinovsky), jahn@earth.sinica.edu.tw (B.M. Jahn), ykatzir@bgu.ac.il (Y. Katzir).

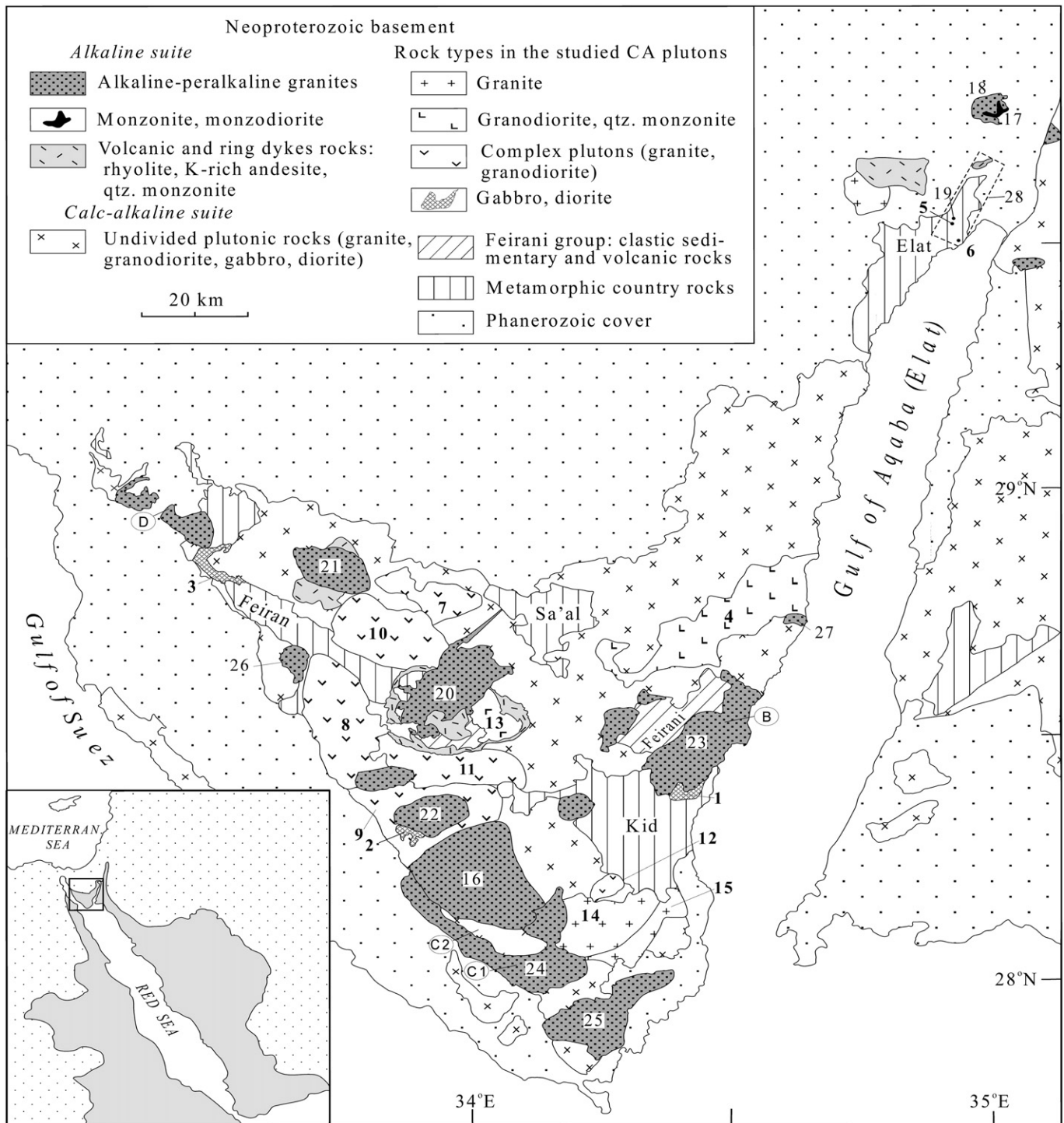


Fig. 1. Sketch map of post-collisional calc-alkaline and alkaline-peralkaline plutonic rocks in the Sinai Peninsula (Egypt) and southern Israel. Compiled on the basis of the Geological map of Sinai 1: 500,000 (Eyal et al., 1980). In the inset, contour of the ANS is shown; also shown is the study area. Studied plutons (numbers correspond to those in Tables 1 and S1): CA suite, early sub-stage: 1 – Shahira; 2 – Imlaha; 3 – Nasrin; 4 – Zreir; 5 – Rehavam; 6 – Nahal Shelomo. CA suite, late sub-stage: 7 – Ahdar; 8 – Hibran-Miar; 9 – Tawla; 10 – Sulaf; 11 – Rahba; 12 – Sama; 13 – Abu Khsheib; 14 – Lathi; 15 – Mandar. Alk suite, early sub-stage: 16 – Gargar, 17 – Timna, monzodiorite; 18 – Timna, alkaline granite; 19 – Yehoshafat. Alk suite, late sub-stage: 20 – Katharina; 21 – Iqna; 22 – Umm-Shomer; 23 – Dahab; 24 – Sahara; 25 – Sharm; 26 – Serbal; 27 – Umm-Ifai; 28 – Elat and Amram areas (S. Israel), in which the bimodal rhyolite-trachydolerite dyke suite was studied (Katzir et al., 2007b). B, C, and D, localities of samples used for the SHRIMP II ion microprobe dating (Ali et al., 2009).

(~820 to 570 Ma) involved vast granitoid magmatism, thought to be well correlated with the changing tectonic setting (Bentor, 1985; Stern and Hedge, 1985; Bentor and Eyal, 1987; Kröner et al., 1990; Stern, 1994; Garfunkel, 1999; Moghazi, 1999, 2002; Jarrar et al., 2003; Katzir et al., 2007b; Jarrar et al., 2008). Four stages of magmatic activity were recognized: (1) island arc magmatism including early

medium-K calc-alkaline plutons (now gneisses) and metavolcanic rocks occurred at ~820–740 Ma; (2) late syn-collisional medium- to high-K calc-alkaline granitoids and gabbro that bear evidence for penetrative deformation and low-grade metamorphism intruded at ~670 Ma to 635 Ma; (3) the most voluminous post-collisional (undeformed) high-K calc-alkaline gabbro-granodiorite-granite

suite formed at ~640 Ma to 620–610 Ma; (4) within-plate alkaline and peralkaline granite suite preceded by intensive bimodal volcanism formed at ~600–550 Ma.

Based on SIMS U–Pb dating of zircon from 24 undeformed plutons in the Sinai Peninsula (Egypt) and southern Israel, Be'eri-Shlevin et al. (2009a) showed that the emplacement of post-collisional calc-alkaline granitoids lasted from c. 635 to 590 Ma, whereas the alkaline granite suite formed during a time span of c. 608–580 Ma. The new geochronological data demonstrate that different granite types that were believed to form in different tectonic settings, were in fact emplaced and crystallized more or less concurrently within the same areas and at the same depth for 20 m.y. long interval. This paper focuses on the provenance of post-collisional granitoid magmas based on chemical and radiogenic isotope composition of rocks from Sinai Peninsula (Egypt) and southern Israel. It complements previous contributions by our team that concentrated on U–Pb geochronological and oxygen isotope data (Be'eri-Shlevin et al., 2009a,b). We present geochemical and radiogenic isotope database of all dated and some undated key plutons from the calc-alkaline and alkaline suites in the northern ANS. The results of our Rb–Sr and Sm–Nd isotope analysis from the Sinai Peninsula and southern Israel are complemented by the published radiogenic isotope data from SW Jordan and the northern Eastern Desert, Egypt. The main objectives of the paper are to: (1) recognize the distinctive chemical features of calc-alkaline and alkaline granites, which are closely spaced and considerably overlap in time; (2) discuss the origin of various granite types in the two suites; (3) to account for coeval emplacement of calc-alkaline and alkaline granitoids in a post-collisional tectonic setting.

2. Geological setting

Three island arcs construct the foundation of the Late Neoproterozoic basement in Sinai Peninsula and southern Israel. From north to south and from old to young they are (Fig. 1):

1. Elat–Feiran island arc comprises the Elat and Feiran groups (Eyal et al., 1980). It extends along the northernmost basement exposures, from the Gulf of Elat in the east almost to the Gulf of Suez in the west. Both groups comprise metapsammitic/metapelitic schist sequences metamorphosed to high amphibolite grade and locally migmatized (Shimron, 1972; Eyal, 1980; Eyal and Amit, 1980; Matthews et al., 1989; Katz et al., 1998, El-Shafei and Kusky, 2003). The age of the protolith of the metasediments is about 820 Ma (Kröner, et al. 1990; Kolodner et al., 2006; Kolodner, 2007).
2. The Sa'al Island Arc is located in the north central part of the basement exposures in Sinai. It is composed of the Sa'al group (Eyal, et al., 1980) including basic to intermediate volcanic rocks and conglomerates metamorphosed at greenschist to low amphibolite facies conditions. The age of Sa'al group is ~740 Ma (Bielski, 1982).
3. The Kid Island Arc is located in the southern part of Sinai. It is composed of the Kid group that includes, in addition to the metavolcanic rocks and metaconglomerate that is predominant in the Sa'al group, also marbles and quartzites (Shimron, 1984). The Kid group was intruded by the Jantil (622 Ma) and Rurabi (632 Ma) granite and diorite plutons (Be'eri-Shlevin et al., 2009b) that were deformed and metamorphosed along with the volcanic and sedimentary rocks. This suggests that deposition of the Kid group occurred prior to ~640 Ma.

The plutonic rocks associated with the island arcs are orthogneisses of tonalite, quartz diorite and monzogranite composition (Stoeser, 1985; Eyal et al., 1991; Cosca et al., 1999; El-Shafei and Kusky, 2003). The metaigneous rocks are thought to represent island arcs at a pre- to syn-collisional tectonic setting, and a subduction-related mechanism for the magma genesis is generally accepted (Stern, 1994; Jarrar et al., 2003).

The island arc stage was followed by collision stage that lasted in Sinai from 640 Ma to 620 Ma in different parts of the region. Collision was associated with extensive uplift, erosion and molasse sedimentation that formed the Feirani group (Eyal, et al., 1980) exposed in Gebel Feirani and Gebel Katharina areas (Fig. 1). It comprises a > 10 km thick section composed of intermediate and acid volcanic rocks, conglomerates and volcanoclastic sediments. The section is metamorphosed at lower greenschist facies conditions only at its base and is folded to big overturned anticlines and synclines. The Feirani Group overlies unconformably the eroded high amphibolite grade rocks of the Kid group, which implies removal of 7 km thick overburden of the Kid group prior to the deposition of Feirani Group (Bentor and Eyal, 1987).

The Late Neoproterozoic calc-alkaline (CA) and alkaline–peralkaline (Alk) igneous rocks that formed during the post-collisional stage occupy about 80% of the exposed basement in Sinai Peninsula and southern Israel (Eyal et al., 1980; Fig. 1). All metasedimentary, metaigneous rocks and the mildly metamorphosed Feirani Group are intruded by the post-collisional granitoids and associated mafic rocks. More than one hundred Late Neoproterozoic plutons have been recognized in the Sinai Peninsula (Bentor and Eyal, 1987). We distinguish plutons *sensu stricto* and plutonic complexes. The plutons are made up of one or several consanguineous rock types with gradational contacts. The plutonic complexes consist of a variety of rock types (e.g., from monzogranite to tonalite and diorite) and occupy larger areas, >200 km². The contact between the different rock types in the complexes may be either sharp or gradational.

During geological mapping CA and Alk granitoids were distinguished based on conventional geological and mineralogical criteria that are similar to those summarized by Liégeois et al. (1998) and Bonin (2004). In particular CA plutons in the study area consist mostly of low-silica granitoids (quartz monzonite, granodiorite, granite with enhanced content of mafic minerals, up to 6–8%); leucocratic granite in complex plutons was classified as calc-alkaline by its gray color, gradational contact with low-silica varieties, and high proportion (~50%) of plagioclase. Common mafic minerals are hornblende and biotite with Mg# = 40–60%; clinopyroxene is more characteristic of diorite and gabbro. The distinctive feature of CA rocks is the common presence of mafic microgranular enclaves (MME) and schlieren, especially in low-silica granitoids.

Alkaline and peralkaline granites were recognized by their pinkish color, high proportion of quartz up to 35–40% (quartz is frequently gray or dark gray), dominance of alkali feldspar over plagioclase or even absence of plagioclase grains, and low abundance of mafic minerals, commonly 1–3% (Fe-rich biotite, hastingsite, and Na-rich amphibole and pyroxene in peralkaline granite). Subordinate quartz syenite is observed in a number of plutons.

Geochemical classification almost always verified the field and mineralogical criteria (see below, Section 4). In individual cases geological–mineralogical features proved to be insufficient for classification of leucocratic granite plutons, and we used the universally accepted discrimination geochemical diagrams and selected Harker diagrams (Figs. 3, 4, 6).

Twenty seven CA and Alk plutons/complexes and one dyke swarm that were studied in detail and characterized by representative sets of chemical analyses are shown in Fig. 1 and discussed below. Most of the plutons have been recently dated by Be'eri-Shlevin et al. (2009a) and Ali et al. (2009). The geological characteristics of the plutons are given in Table 1. In each pluton/complex the rock types are listed in the order of decreasing abundance.

The rocks of the CA suite vary from gabbro to leucocratic granite. The main rock types are granodiorite and monzogranite with subordinate quartz monzonite, tonalite, diorite, quartz diorite, and gabbro. The mineralogical and chemical compositions of the CA granitoids allow classifying them as I-type granites.

Granites of the Alk suite were studied in 16 plutons ranging in size from 1 to 400 km² (Fig. 1; Table 1). Some of them are central plutons

Table 1
Characteristics of studied plutons and complexes.

Pluton and complex name	No. in Fig. 1	Location in Sinai	Exposed area, km ²	Isotopic age, Ma	Rock type arranged according to decreasing abundance. In parentheses are mafic minerals	Color index vol.%	Amount of counted samples	Geological and structural features
<i>Calc-alkaline suite, early stage</i>								
Basic plutons								
Shahira	1	Central E	14	632 ± 4 [¹]	Gabbro (hbl) Gabbro (bi, hb)	28–55 20–54	24	A layered gabbro intrusion that is clearly exhibited mainly in the western part.
Imlaha	2	Central W	16	~630	Granodiorite (bi, hbl) Qz. diorite (hbl) diorite (hbl) Qz. monzodiorite (hbl)	12–18 33–47 48–60 45	8	Different rock types make up irregular patches of few tens to few hundred meter across, mostly with gradational contacts between the patches. The pluton is intruded by the Tawla complex (No 7) and Umm-Shomer pluton (No 22).
Nasrin	3	NW	33	~630	gabbro (hbl) Gabbro (bi, hbl) Gabbro (hbl) Gabbro (bi)	53 32–46 15–65 37	13	The pluton is a homogeneous intrusive body. It intrudes the metamorphic rocks of Feiran Group.
Granodiorite and granite plutons								
Zreir complex	4	Central E	E. – 180 W. – 120 Tot – 300	629 ± 6 [¹]	Granodiorite (hbl, bi) Monzogranite (hbl, bi) Qz monzodiorite (hbl, bi) Qz diorite (hbl, bi) Tonalite (bi, hbl)	10–29 9–13 15–21 20–30 13	21	The dioritic and granitic rocks make up different (eastern and western) parts of the pluton. All rock types contain microgranular mafic enclaves (MME) with increasing amount in the more basic rocks. The eastern end of the pluton is faulted in the Gulf of Elat.
Rehavam	5	NE	3	630 ± 5 [¹]	Monzogranite (bi, ms ± grt) [²]	4–6	6	The Rehavam and Nahal Shelomo plutons are only few km apart. In the Nahal Shelomo pluton its upper part is exposed with abundant pegmatites and aplitic veins, whereas the Rehavam pluton is deeply eroded [²]
Nahal Shelomo	6	NE	1	636 ± 8 [¹]	Monzogranite (bi, ms) [²]	5–8	7	
<i>Calc-alkaline suite, late stage</i>								
Complex plutons								
Ahdar complex	7	Central N	213	610 ± 5 [¹]	Granodiorite (hbl, bi) Monzogranite (hbl, bi) Monzogranite (bi) Qz diorite (bi, hbl)	9–16 6–11 1–5 12	11	The complex contains large relicts (stopped blocks) of the Feiran Group country rocks (mainly schist). MME are common in all rock types
Hibran-Miar complex	8	Central N	Diorite 91 granodior. 141	619 ± 4 [¹]	Granodiorite (hbl, bi) Monzogranite (hbl bi/bi) Qz diorite (hbl, bi/bi, hbl) Tonalite (hbl, bi/bi, hbl) Qz monzodiorite (hbl bi/bi) Diorite (hbl) Syenogranite (hbl, bi)	7–24 2–11 22–45 20–33 7–17 38 2	46	The complex is composed of dioritic and granitic rocks. The diorite and granitoids form separate areas of few km ² in size. All rock types contain MME.
Tawla complex	9	Central N	111		Granodiorite (hbl, bi/bi, hbl) Monzogranite (hbl, bi/bi, hbl) Qz monzodiorite (hbl, bi/bi, hbl) Qz monzonite (bi) tonalite (hbl, bi)	6–20 5–9 3–17 5 9	23	Various rock types are distributed irregularly within the complex, contacts are mostly gradational. MME are common, their proportion is higher in the more basic rocks. The SW part of the complex is faulted down in the Gulf of Suez graben. The Tawla Complex intrudes the Imlaha pluton (No 1) and is intruded by the Umm-Shomer pluton (No 22).
Sulaf complex	10	Central N	252	597 ± 5 [¹]	Granodiorite (bi/hbl, bi) Qz diorite (hbl, bi) Tonalite (hbl, bi) Qz monzodiorite (bi) Monzogranite (bi)	3–10 4–18 4–20 8–10 2–3	14	The complex consists mainly of granitoids and less of dioritic rocks. The monzogranite and more leucocratic granodiorite do not contain MME, whereas in diorite and melanocratic granodiorite MME are common. The contacts between the different rock types are gradational, in places sharp. The Sulaf complex is intruded by plutonic and dyke rocks of the Katharina ring complex (No 20).

Granodiorite plutons								
Rahba	11	Central N	75	610 ± 5 [1]	Granodiorite (hbl, bi)	10	4	Granodiorite contains abundant MME, many of them show different stages of hybridization by the host granitic magma. The pluton is intruded by the Katharina Ring Dike (No 20). The pluton is made up mostly of granitoids; monzodiorite occurs sporadically. MME are common, in more basic rocks they are abundant. Clear evidence of hybridization of enclaves up to schlieren formation is widely exhibited [3].
Sama	12	SE	12	608 ± 4 [1]	Qz monzonite (hbl, bi) Monzogranite (hbl, bi) Granodiorite (hbl, bi) Monzodiorite (hbl, bi) [3]	5–9 5–8 11 7	8	
Abu Khsheib	13	Central N.	82	592 ± 7 [1]	Qz monzonite (hbl, bi) Monzodiorite (hbl, bi) Granodiorite (hbl, bi)	6–9 4–8 7	5	
Granite plutons								
Lathi	14	SE	167	607 ± 4 [1]	Monzogranite (bi/hbl, bi) Granodiorite (hbl, bi) Qz monzodiorite (hbl, bi) [3]	4–10 7 13	12	Within the outer zone of the pluton, less than 1 km wide, the rock contains MME and becomes porphyritic with plagioclase phenocrysts and enriched in mafic minerals [3]. The Mandar pluton is composed of very homogenous coarse-grained rock. It intrudes the Lathi pluton (No 14). [3]
Mandar	15	SE	90	604 ± 4 [1]	Monzogranite (bi) Syenogranite (bi) [3]	1–6 1–4	11	
Alkaline suite, early stage								
Girgar	16	SW	400	603 ± 4 [1]	Syenogranite (bi/hbl, bi) Monzogranite (bi/hbl, bi) [3]	2–4 2–5	10	The pluton is composed of very homogenous medium- to coarse-grained rock. It is intruded by the Sahara pluton (No 24). Rock compositions change on short distances. MME (10–30 cm) are common. Mafic rocks are intruded by the Timna Alkaline Granite (No 18).
Timna Monzodiorite	17	NE	4	602 ± 5 [1]	Monzodiorite (hbl, bi) Monzonite (hbl, bi) Qz monzodiorite (bi, hbl) Diorite (hbl, bi) [6]	33 24 22 59		
Timna Alkaline Granite	18	NE	10	606 ± 3 [1] 609 ± 10 [5]	Syenogranite (bi) [6]	2–4		Timna Alkaline Granite intrudes Timna Monzodiorite (No 17).
Yehoshafat	19	NE	0.8	605 ± 4 [1]	Syenogranite (bi)	3	7	The homogenous stock-like pluton intrudes the Rehavam pluton (No 6) and early andesite dikes
Alkaline suite, late stage								
Syenogranite and monzogranite plutons								
Katharina	20	Central N.	220	583 ± 6 [1]	Monzogranite (bi) Syenogranite (bi) Alkali feldspar granite (bi) [8]	1–5 2–4 2–7	110	The pluton is situated in the central part of the Katharina ring complex. It is zoned with monzogranite and syenogranite as the main body whereas the alkali feldspar granite forms the uppermost part with a gradational contact with syenogranite [7, 8]. The pluton is part of the Iqna ring complex. It is exposed from the roof to few hundred meter inward the pluton.
Iqna	21	NW	109	594 ± 6 [1] 578 ± 8 [1]	Monzogranite (bi) Syenogranite (bi) Alkali feldspar granite (bi)	2–8 1–5 2	11	
Umm-Shomer	22	Central W	80	596 ± 5 [1]	Syenogranite (bi)	1–3.5	7	
Dahab	23 B	Central E	170	591 ± 6 [1] 594 ± 8 [11]	Monzogranite (bi, hrb/bi) Syenogranite (bi, hrb/bi) Alkali feldspar granite (bi, hrb)	6–18 3–16 7	22	
Peralkaline and alkali feldspar granite plutons								
Sahara	24	S	250	608 ± 56 [1] 579 ± 9 [11]	Alkali granite (rieb)	0.5–7	9	It is a deeply eroded ring dike of an ellipsoid shape with axes of 25 and 40 km and maximum width of 9 km. It intrudes the alkaline Girgar pluton (604 Ma) and the calc-alkaline monzogranite pluton emplaced ~594 Ma [3, 12]. Granite and syenite contain abundant hybridized xenoliths ~10 cm in diameter and large stopped blocks of the Kid Group rocks up to few hundred meter across [3, 9].
Sharm	25	S	200	594 ± 4 [1]	Alkali feldsp. granite (hrb/bi, hrb) Alkali feldsp. Qz syenite (hrb/bi, hrb) and syenite (hrb)	3–10 5–14 10	18	
Serbal	26	NW	40		Alkali feldspar granite (hrb) Syenogranite (bi)	1.5–4 4	4	

(continued on next page)

Table 1 (continued)

Pluton and complex name	No. in Fig. 1	Location in Sinai	Exposed area, km ²	Isotopic age, Ma	Rock type arranged according to decreasing abundance. In parentheses are mafic minerals	Color index vol.%	Amount of counted samples	Geological and structural features
<i>Peralkaline and alkali feldspar granite plutons</i>								
Umm-Ifai	27	Central E	13	586 ± 4 [1]	Syenogranite (bi) Monzogranite (bi) Alkali feldspar granite (bi) Peralkaline granite (rieb, bi)	4–5 2–3 1.5 2	7	The alkali and alkali feldspar granite occur mainly in the eastern part of the pluton, whereas the syenogranite and monzogranite are abundant in the western part. No sharp contact was found. The eastern part of the pluton is faulted down in the Gulf of Elat.
Wadi Seih	D	NE		591 ± 6 [1]	Peralkaline granite			Outcrop of peralkaline granite of 1.5 by 2 km [11]
Bimodal dyke suite	28	NE		593 ± 6 [10] 594 ± 8 [10]	Porphyritic rhyolite (bi) Trachydolerite (cpx) Trachyandesite(cpx, bt)	2–3 25–30 30	15	Rhyolite comprises about 95% of the dykes; their thickness attains 20–25 m. Mafic rocks compose marginal zones in abundant composite dykes [10].

Notes:

1. Isotopic ages were determined by the U–Pb dating in zircon; ~estimated age based on field evidence and similarity in rock compositions.

2. In the second column the pluton/complex number as in Fig. 1 and Table S1.

3. Rock types were distinguished based on their modal mineral composition.

4. Literary sources: [1] Be'eri-Shlevin et al., 2009a; [2] Eyal et al., 2004; [3] Bentor and Eyal, 1987; [4] Bielski, 1982; [5] Beyth et al., 1994; [6] Shpitzer et al., 1992; [7] Katzir et al., 2007a; [8] Eyal and Hezkiyahu, 1980; [9] Bentor, 1985; [10] Katzir et al., 2007b; [11] Ali et al., 2009.

in ring complexes best exhibited in the Katharina ring complex (Eyal and Hezkiyahu, 1980; Katzir et al., 2007a). Volcanic rocks that preceded the emplacement of alkaline granite form the Katharina group of rhyolite and ignimbrite, with secondary trachyandesite; the sedimentary rocks are conglomerates. In the ring complexes granite is intrusive into volcanic rocks and ring dykes and often shows miarolitic texture, indicating crystallization at shallow depth.

The majority of Alk plutons are composed of syenogranite, alkali feldspar and peralkaline granite (Table 1). The only pluton in the region made up solely of peralkaline riebeckite granite is the Sahara pluton. Contacts between various granite types are mostly gradational. Related mafic rocks were described only in the Timna Monzodiorite pluton and in composite dykes made up of trachydolerite and alkali feldspar rhyolite (Beyth et al., 1994; Mushkin et al., 2003; Katzir et al., 2006, 2007b). Unlike CA granitoids MME are not characteristic of the Alk suite. The exception is the Dahab pluton with rare MME and fine-grained clusters enriched in biotite, amphibole and plagioclase.

The ages of the CA and Alk igneous rocks given in Table 1 are mostly after Be'eri-Shlevin et al. (2009b) supplemented by data from Ali et al. (2009). Emplacement of CA plutons lasted from 636 ± 8 Ma (Nahal Shelomo) to 592 ± 7 Ma (Abu Khsheib). The alkaline magmatism started at 606 ± 3 Ma (Timna), and was in progress till 578 ± 8 Ma (Iqna), so that CA and Alk magmas in the studied region were emplaced concurrently during a period of ~20 m.y. However, in each particular area alkaline granites are younger than calc-alkaline ones. Thus in central southern Sinai, the calc-alkaline Abu Khsheib pluton (592 ± 7 Ma; number 13 in Table 1 and Fig. 1) is intruded by the alkaline Katharina pluton (583 ± 6 Ma; number 20). In Southern Israel the Timna alkaline granite (606 ± 3 Ma; number 18) was injected in porphyritic CA granite dated at 625 Ma (Beyth et al., 1994); and the alkaline Yehoshafat granite (605 ± 6 Ma; number 19) intrudes the CA granite of the Rehavam pluton (630 ± 6 Ma; number 5), see Eyal et al. (2004).

In almost all cases the agreement between ion-probe U–Pb ages and field relations was satisfactory or even perfect (Table 2 and Table 1-SD in Supplementary data). The sole debatable issue is the age of the Sahara pluton determined by Be'eri-Shlevin et al. (2009a) at 608 ± 5 Ma and by Ali et al. (2009) at 579 ± 9 Ma. The second estimate seems more realistic since it is consistent with the field relations and U–Pb zircon age of the Girgar (603 ± 4 Ma) and the unnamed CA monzogranite pluton (594 ± 14 Ma; Ali et al., 2009, location C2 in Fig. 1), both intruded by the Sahara pluton (Fig. 1).

Two sub-stages of emplacement can be distinguished in each suite (Table 1). An early sub-stage in the CA suite, 635–615 Ma, included the emplacement of gabbro, diorite and two-mica granite, whereas highly fractionated biotite granite (Mandar and Lathi plutons) intruded in the later sub-stage (610–590 Ma). However, the most abundant CA granodiorite–granite plutonic complexes occur in both sub-stages.

In the Alk suite a division to two sub-stages is more obvious. During the early sub-stage (~610–600 Ma) only syenogranite plutons were emplaced; in the Timna complex the syenogranite was preceded by monzodiorite. The onset of the later Alk sub-stage (~600–580 Ma) was heralded by extensive volcanic activity in the Katharina and Iqna ring complexes (central Sinai), emplacement of alkaline and peralkaline granites and abundant injection of alkali feldspar rhyolite dyke swarms (Katzir et al., 2006, 2007b). Notably the later, felsic sub-stage of the CA suite and the early, syenogranitic sub-stage of the Alk suite started almost simultaneously, at 610–608 Ma.

3. Analytical methods

3.1. Whole-rock chemical analysis

Whole-rock chemical analysis was performed at the Geological Survey of Israel by ICP-AES (Perkin-Elmer; Elan 3000) for major elements and by ICP-MS (Perkin-Elmer; Elan 6000) for trace elements (Rb, Sr, Ba, Y, Zr and Nb) and REE. For major element analysis rock

powders (0.5 g per sample) were melted with $\text{Li}_2\text{B}_2\text{O}_4$ (1.25 g) in platinum crucibles and the melt was dissolved in 0.1 N HNO_3 . A 5 ppm aliquot of an internal Sc standard was added to each dissolved sample. For trace element analysis rock powders (0.5 g) were sintered with Na_2O_2 (2 g) in zirconia crucibles at 500 °C followed by dissolution in 2 N HNO_3 . An internal standard solution of 10 ppb Rh + Re was added to each sample. International standards SO-3, NIM-G, NIM-L, BCR-32 and BHVO-1 were routinely measured during ICP-AES analysis. Likewise ICP-MS measurements were standardized using SO-3 and JB-1. The results of the standards SO-3 and NIM-G analysis are given in Table 2. Whole-rock chemical analysis of major elements in selected samples was performed at the Geological Institute of the Russian Academy of Sciences (Ulan-Ude) using a combination of photometry (SiO_2 , TiO_2 , Al_2O_3 , P_2O_5), flame emission spectrometry (Fe_2O_3 , MgO, CaO) and titration (FeO). In Table 2 the result of analysis of the standard NIM-G is shown. Analyses are considered accurate to within 2–5% for major elements, and better than 10–15% for trace elements. The accuracy for all the REE (except Lu) is 1–5%; for Lu, it is 9–10%.

Additionally REE contents of 26 samples were measured by ICP-MS (Agilent 7500s) at the National Taiwan University (NTU), Taipei. Rock powders were first fused to make glass beads for XRF major element determination. Used glass beads were then powdered and dissolved in HF/ HNO_3 (1:1) mixture in capped Savilex beakers for >2 h at ca. 100 °C, followed by evaporation to dryness, refluxing in 7 N HNO_3 for >12 h at ca. 100 °C and finally, diluting the sample solution by 2% HNO_3 . An internal standard solution of 5 ppb Rh and Bi was added and the spiked solution was diluted with 2% HNO_3 to a sample/solution weight ratio of 1:2000. The precision was generally better than $\pm 5\%$ (2-sigma) for most trace elements, as shown by the statistics of duplicate analyses on five rock standards AGV-1, AGV-2, GSP-1, JB-1 and JG-1 (Yang et al., 2005; see Appendix, Table A). The results of analysis of the international standards (=AGV-1, AGV-2, GSP-1, JB-1 and JG-1) are also given in the Appendix of the cited paper.

3.2. Rb–Sr and Sm–Nd isotope analyses

Sr and Nd isotope ratios were measured using a Finnigan MAT-262 thermal ionization mass spectrometer at the Institute of Earth Sciences (IES), Academia Sinica, Taipei. Concentrations of Rb, Sr, Sm and Nd were determined by ICP-MS at the National Taiwan University (see above for the analytical procedure).

Sr and Nd isotope ratios were measured on unspiked samples. Powdered samples were dissolved in Savilex bombs and followed by a series of standard procedures until samples were completely dissolved. Isolation of Sr and Nd were achieved using a 2-column technique, and Sr fractions were occasionally further purified using a third column. The first column was packed with 2.5 ml cation exchange resin (Bio-Rad AG50W-X8, 100–200 mesh) and was used to collect Sr and REE fractions. The second column used for Sr purification was packed with 1 ml cation exchange resin, identical to the above. The second column used for Nd isolation was packed with 1 ml Ln-B25-A (Eichron) resin, which was covered on top by a thin layer of anion exchange resin (Bio-Rad AG1-X8, 200–400 mesh).

Mass analyses were performed using a 7-collector Finnigan MAT-262 mass spectrometer in dynamic mode. $^{143}\text{Nd}/^{144}\text{Nd}$ ratios were normalized against the value of $^{146}\text{Nd}/^{144}\text{Nd} = 0.7219$, whereas $^{87}\text{Sr}/^{86}\text{Sr}$ ratios were normalized to $^{86}\text{Sr}/^{88}\text{Sr} = 0.1194$. During the course of analyses, measurements on NBS-987 Sr standard yielded $^{87}\text{Sr}/^{86}\text{Sr} = 0.710320 \pm 0.000036$ ($n = 50$) using static mode and $= 0.710237 \pm 0.000020$ ($n = 8$) using dynamic mode. The $^{87}\text{Sr}/^{86}\text{Sr}$ ratios reported herein (Table 4) have been duly adjusted to NBS-987 = 0.710250. Our measurements on La Jolla Nd standard yielded 0.511864 ± 0.000006 ($n = 4$), and on JMC Nd standard, 0.511821 ± 0.000016 ($n = 6$). The one-stage model age ($T_{\text{DM-1}}$) is calculated

Table 2
Chemical composition (wt.%, ppm) of igneous rocks from the CA and Alk suites (S. Israel and Sinai Peninsula, Egypt).

Suite	Calc-alkaline, stage 1										
	Shahira (1)		Imlaha (2)	Nasrin (3)		Zreir (4)			Rehavam (5)		
Pluton/complex	Shahira (1)		Imlaha (2)	Nasrin (3)		Zreir (4)			Rehavam (5)		
Sample no.	S-3905	[S-3807]	S-2330	S-2847**	S-2839**	S-4585	S-4563**	S-4586	[S-4577]	A44**	A39**
Rock type	Gbr	GD	Gbr	Gbr	Gbr	Q-MnzD	GD	Gr	Gr	Gr	Gr
Latitude N	28°21'47"	28°24'14"	28°16'14"	28°48'38"	28°50'00"	28°49'00"	28°48'39"	28°48'52"	28°48'09"	29°35'28"	29°32'52"
Longitude E	34°21'54"	34°22'09"	33°51'45"	33°29'35"	33°28'45"	34°33'06"	34°37'15"	34°32'41"	34°30'55"	34°57'33"	34°54'07"
SiO ₂	46.5	65.5	48.0	53.2	49.0	63.6	65.7	68.2	69.5	74.0	73.7
TiO ₂	1.3	0.92	1.55	1.05	1.63	0.65	0.62	0.45	0.35	0.13	0.15
Al ₂ O ₃	19.0	15.5	17.5	17.8	17.7	16.2	15.6	15.6	15.0	15.0	14.4
Fe ₂ O ₃	6.32	2.55	12.3*	8.5*	10.5*	2.06	2.41	1.8	1.6	0.12	0.68
FeO	6.1	2.2				2.28	1.61	0.72	0.72	0.91	0.44
MnO	0.12	0.08	0.18	0.14	0.14	0.07	0.06	0.04	0.04	0.04	0.04
MgO	5.6	2.4	6.0	5.1	5.5	2.4	2.1	1.5	1.3	0.26	0.32
CaO	11.0	4	9.0	7.7	8.5	4.2	3.2	2.7	2.4	1.15	1.1
Na ₂ O	2.50	3.7	2.90	3.2	3.70	3.80	4.1	4.50	4.1	4.78	4.68
K ₂ O	0.50	2.9	1.30	1.4	1.20	2.90	3.4	3.60	3.6	3.25	3.45
P ₂ O ₅	0.1	0.2	0.11	0.2	0.3	0.2	0.2	0.1	0.05	0.04	0.05
LOI	0.80	0.6	1.70	1.6	1.60	0.70	0.5	0.40	0.5	0.51	0.65
Total	99.74	100.55	100.54	99.89	99.77	99.07	99.5	99.61	99.16	100.19	99.66
Rb	7	71	30	45	30	90	95	105	90	84	80
Sr	836	595	641	616	904	431	712	703	649	390	390
Ba	210	1430	250	389	465	616	917	966	889	500	500
Nb	4	14		7	8	10	10	8	7	9	6
Th	1.6	5.9		2.9	3.2	7.4	11	12.6	11		
U	0.60	1.60		1.7	1.10	2.90	3.15	3.90	1.65		
Pb		15		20	20		40	45	20		
Zr	80	265	40	75	85	120	160	150	110	70	70
Hf	1.6	1.4		2	2.0	2.0	1.6	1.8	1.8		
Y	11	22	20	13	20	18	11	8	7	11	8
Ga	25	24		18	20	22	22	22	20		
La	8	38	10	15	21	22	24	26	19	6	8
Ce	18	83	25	32	50	46	50	52	38	19	26
Pr	2.5	9.8	4.0	4	6.4	5.6	5.5	5.8	4.3	1.5	2.4
Nd	11	36	17	19.2	29	22	21	20	15	6	9
Sm	3.1	6.9	4.9	4.33	6.7	4.7	3.47	3.6	2.5	1.4	2.1
Eu	0.86	1.46	1.40	1.3	1.94	0.98	1.0	0.94	0.70	0.37	0.50
Gd	2.4	5.0	3.8	3.85	6.0	3.8	2.85	2.4	1.8	1.3	1.7
Tb	0.40	0.74	0.63	0.58	0.80	0.58	0.38	0.38	0.26	0.22	0.25
Dy	2.3	3.85	3.6	3.1	4.1	3.4	1.88	1.7	1.3	1.2	1.3
Ho	0.44	0.80	0.80	0.61	0.80	0.62	0.38	0.32	0.22	0.24	0.25
Er	1.25	2.10	2.02	1.64	2.20	2.00	1.06	0.85	0.55	0.68	0.67
Tm	0.18	0.30	0.29	0.23	0.30	0.30	0.15	0.12	0.09	0.11	0.10
Yb	1.05	2.0	1.65	1.45	1.85	1.75	1.0	0.75	0.55	0.72	0.68
Lu	0.12	0.26	0.25	0.2	0.24	0.24	0.16	0.10	0.07	0.10	0.10
Eu/Eu*	0.98	0.77	1.01	0.99	0.95	0.72	0.96	0.99	1.02	0.84	0.82
(La/Yb) _n	5.0	12.5	4.0	6.8	7.3	8.3	15.2	23.2	23.2	5.0	8.1
NK/A		0.59				0.58	0.67	0.72	0.71	0.76	0.79
A/CNK		0.94				0.95	0.96	0.96	1.0	1.11	1.07

(1) In parentheses near the pluton's name are their numbers in Fig. 1 and Table 1.

(2) In brackets are samples used for the U–Pb dating. ** Samples analysed for Sr–Nd isotopes.

(3) Abbreviations: Gbr = gabbro; GD = granodiorite; Q-MnzD = quartz monzodiorite; Q-Mnz = quartz monzonite; Gr = granite; Afs Gr = alkali-feldspar granite; Q-Afs SY = quartz alkali-feldspar syenite; PA Gr = peralkaline granite; Mnz = monzonite; Tdol = trachydolerite; QP = quartz porphyry.

(4) 12.3* = total Fe calculated as Fe₂O₃.

(5) Hyphen = concentration of element below the detection limit.

(6) $Eu/Eu^* = Eu_n / (Sm_n + Gd_n)^{1/2}$; $NK/A = (Na_2O + K_2O) / Al_2O_3$, $A/CNK = Al_2O_3 / (CaO + Na_2O + K_2O)$, mol%.

(7) Rock compositions from the Timna Complex after Beyth et al. (1994).

(8) In the end of the table the results of analysis of the standards SO-3 and NIM-G are given. Lab-1, Geological Survey of Israel (ICP-AES, ICP-MS), averages of three measurements; Lab-2, Geol. Institute, Ulan-Ude, Russia; averages of five measurements ($2\delta \leq 5\%$ for major and REE and 10–15% for trace elements).

assuming a linear Nd isotopic growth of the depleted mantle reservoir from $\epsilon_{Nd(T)} = 0$ at 4.56 Ga to +10 at the present time.

$$T_{DM-1} = 1/\lambda \ln \left\{ 1 + \left[\frac{^{143}Nd}{^{144}Nd} s - 0.51315 \right] \div \left[\frac{^{147}Sm}{^{144}Nd} s - 0.2137 \right] \right\},$$

where s = sample, λ = decay constant of ^{147}Sm (0.00654 Ga^{-1}).

The two-stage model age (T_{DM-2}) is obtained assuming that the protolith of the granitic magmas has a Sm/Nd ratio (or $f_{Sm/Nd}$ value) of

the average continental crust (Keto and Jacobsen, 1987):

$$T_{DM-2} = T_{DM1} - (T_{DM1} - t)(fcc - fs) / (fcc - f_{DM}),$$

where f_{cc} , f_s , $f_{DM} = f_{Sm/Nd}$ are values of the average continental crust, the sample and the depleted mantle, respectively. In our calculation, $f_{cc} = -0.4$ and $f_{DM} = 0.08592$ are used, and t = the intrusive age of granite.

Calc-alkaline, stage 2										
	N.Shelomo (6)		Ahdar (7)		H-Miar (8)		Tawla (9)		Sulaf (10)	
A102	A29	A4	S-2902**	S-2911**	S-1996	[S-2351]	S-1955	S-1953	S-2109	[S-2199]
Gr	Gr	Gr	GD	Gr	Gr	Gbr	Gr	Gr	Q-Mnz	Q-MnzD
29°33'27"	29°31'41"	29°32'19"	28°46'32"	28°45'38"	28°35'04"	28°25'37"	28°20'50"	28°20'15"	28°42'46"	28°39'44"
34°54'15"	34°54'54"	34°55'17"	33°45'56"	33°47'05"	33°45'18"	33°42'07"	33°58'50"	33°59'14"	33°44'00"	33°45'45"
72.8	74.7	75.4	66.7	70.9	72.3	51.0	68.0	70.3	66.7	60.3
0.14	0.15	0.15	0.4	0.3	0.39	1.47	0.5	0.3	0.5	0.6
14.5	13.5	13.4	15.9	14.7	14.4	19.0	15.9	14.6	16.1	19.8
0.73	0.76	0.3	3.6*	2.7*	2.7*	9.8*	3.1*	2.3*	3.5*	4.9*
0.43	0.84	1.24								
0.04	0.03	0.03	0.07	0.07	0.05	0.13	0.08	0.06	0.06	0.08
0.52	0.21	0.19	1.5	0.9	0.9	4.5	0.9	0.7	1.2	1.6
0.78	0.48	1.18	3.0	2.0	1.6	7.1	2.3	2.0	3	4.1
5.20	4.30	3.82	4.30	4.00	3.50	4.2	4.30	3.60	4.70	5.7
3.34	3.77	3.76	2.80	3.70	3.90	1.7	4.20	4.60	3.30	2.3
0.06	0.04	0.05	0.2	0.1	0.1	0.39	0.2	0.1	0.1	0.3
0.88	1.19	0.73	0.80	0.20	0.70	2.0	0.50	0.40	0.70	0.6
99.42	99.97	100.25	99.27	99.57	100.54	101.29	99.98	98.96	99.86	100.28
93	110	105	80	125	120	38	100	96	80	62
360	92	98	434	258	302	913	310	255	392	661
450	550	600	608	389	700	600	1041	632	716	846
8	10	10	10	14	14	9	17	13	11	9
4.4	8.8	7.1	7.6	12.9	20.0	2.2	9.0	13.7	9.0	5.5
4.11	1.30	1.04	2.85	3.85	4.10	0.65	2.00	2.40	1.80	1.65
15	14	14	35	20	15	20	20	20	60	25
70	120	100	200	200	100	80			250	500
2.2	2.7	1.9	2.4	2.8	3.2	1.2	1.4	1.8	2.0	3
12	8	8	11	17	23	25	32	19	15	9
21	21	18	18	16	16	19	17	15	15	19
13	24	22	28	22	35	22	35	38	26	27
28	50	45	55	44	72	53	82	65	52	53
3.2	5.6	5.0	6.1	5.1	6.2	6.9	9.8	6.5	5.2	5.5
12	20	17	23	20	23	30	40	24	22	20
2.4	3.7	3.0	4.0	4.0	4.4	6.2	7.9	4.6	3.9	3.3
0.56	0.50	0.52	1.01	0.71	0.96	2.02	1.78	1.08	1.16	1.82
2.1	3.1	2.5	3.5	3.6	3.4	5.8	6.4	3.8	3.4	2.4
0.34	0.42	0.34	0.48	0.56	0.58	0.88	0.98	0.62	0.56	0.40
2.1	1.9	1.52	2.4	3.1	2.9	4.4	5.5	3.3	2.6	1.55
0.46	0.30	0.24	0.48	0.64	0.62	0.84	1.10	0.70	0.54	0.32
1.17	0.73	0.61	1.35	1.85	1.70	2.40	3.10	1.95	1.55	0.99
0.18	0.09	0.08	0.20	0.29	0.26	0.36	0.50	0.32	0.24	0.14
1.19	0.63	0.54	1.34	2.01	2.00	2.10	3.00	2.00	1.50	0.90
0.17	0.11	0.09	0.21	0.31	0.20	0.26	0.40	0.26	0.22	0.12
0.77	0.46	0.58	0.84	0.58	0.77	1.04	0.78	0.80	0.99	2.02
7.1	25.4	27.0	13.8	7.3	11.5	6.9	7.7	12.4	11.5	19.7
0.84	0.83	0.77	0.64	0.72	0.69	0.46	0.73	0.75	0.7	0.6
1.07	1.12	1.07	1.02	1.03	1.12	0.88	1.01	1	0.96	1.03

4. Chemical composition

The complete geochemical dataset contains more than 200 analyses. Of them, about 40% of the CA granitoid and mafic rock samples have positive Eu anomalies ($\text{Eu}/\text{Eu}^* \geq 1.0$), which indicate the presence of cumulate feldspar crystals (Fig. 1-SD, online version, [Supplementary data](#)). Cumulus-rich samples misrepresent the bulk magma composition. This is illustrated by a set of granite samples from complex plutons (Fig. 2-SD, [Supplementary data](#)): increase of the Eu/Eu^* value from 1.0 to 2.54 is associated with progressive

decrease in REE, Th, U, Nb, Y and increase in Sr content of the rocks. Therefore, all samples with $\text{Eu}/\text{Eu}^* > 1.1$ have been excluded from further consideration of the original bulk magma composition. Also excluded were samples of gabbro and diorite with low Al_2O_3 (~11 wt.%) and anomalously high MgO, CaO and FeO^t , because such features indicate abundant mafic crystal cumulates. The present discussion on the geochemistry of the plutonic rocks is based on 171 analyses. Chemical compositions of the 69 most representative samples are given in Table 2, and the whole dataset may be seen in Table 1-SD (online version; [Supplementary data](#)).

Table 2 (continued)

Suite	Calc-alkaline, stage 2										
	Rahba (11)		Sama (12)			Abu-Khsheib (13)		Lathi (14)			Mandar (15)
Pluton/Complex											
Sample no.	S-1876	[S-2069]	S-3700	S-3706	[S-3704]	S-2676	[S-2695]	S-1701	S-1617**	[S-1610]	S-1714
Rock type	Gr	Gr	Q-Mnz	Gr	Gr	Q-Mnz	Gr	Gr	Gr	Q-MnzD	Gr
Latitude N	28°23'30"	28°26'16"	28°11'24"	28°11'14"	28°11'08"	28°29'53"	28°32'12"	28°07'08"	28°03'52"	28°08'00"	28°02'57"
Longitude E	34°00'39"	33°52'32"	34°13'47"	34°15'34"	34°16'06"	34°02'32"	34°03'43"	34°14'56"	34°10'07"	34°10'16"	34°16'24"
SiO ₂	67.0	72.3	65.5	71.8	69.0	66.1	68.0	70.25	72.0	61.50	73.0
TiO ₂	0.5	0.3	0.63	0.36	0.51	0.7	0.6	0.5	0.42	0.81	0.33
Al ₂ O ₃	15.8	14.5	16.9	14.8	15.70	15.7	15.1	14.91	14.7	17.7	14.1
Fe ₂ O ₃	3.6*	2.0*	2.94	2.13	2.17	4.2*	3.5*	1.42	1.64	3.83	1.73
FeO			0.59	0.06	0.93			0.8	0.51	1.23	0.06
MnO	0.07	0.02	0.09	0.07	0.09	0.1	0.06	0.07	0.06	0.1	0.05
MgO	1.2	0.5	1.3	0.6	1.10	1.3	1.1	0.53	0.7	1.6	0.6
CaO	2.8	1.8	2.7	1.4	2.30	2.9	2.5	1.02	1.7	4.1	1.5
Na ₂ O	4.30	3.30	4.80	4.10	4.30	4.70	4.50	3.92	3.7	4.8	3.80
K ₂ O	3.60	4.60	3.40	3.90	3.50	3.50	3.70	5.81	3.6	2.4	3.70
P ₂ O ₅	0.1	0.05	0.1	-	-	0.3	0.3	0.09	-	0.2	-
LOI	0.50	0.40	0.70	0.40	0.40			0.38	0.50	1.2	0.40
Total	99.47	99.77	99.65	99.62	100.0	100.1	100.16	99.70	99.52	99.47	99.27
Rb	105	170	68	99	76	85	100	78	104	48	109
Sr	402	234	437	218	317	428	394	278	245	607	210
Ba	742	596	1290	732	1040	728	673	745	878	1120	673
Nb	13	15	13	14	14	15	15	13	13	16	15
Th	10.5	27.6	6.2	13.5	9.7	12.1	14.1	5.6	8.65	6.7	18.0
U	1.75	6.40	1.90	5.30	2.55	3.15	3.80	1.75	3.60	2.30	4.20
Pb	20	25		25	35	45	20	17	40	10	5
Zr	310	200			310	290	240	130	180	370	160
Hf	1.6	3.4	0.6	2.6	2.2	2.8	2.8	2.0	1.8	1.6	2.8
Y	17	18	27	24	25	22	19	27	27	28	16
Ga	18	14	19	19	19	17	17	15	18	20	15
La	31	38	35	38	36	37	37	25	24	30	35
Ce	65	74	82	76	79	78	74	66	78	66	72
Pr	7.0	6.8	9.9	8.1	9.2	8.6	8.4	8.5	8.2	7.8	7.4
Nd	28	24	39	30	34	32	32	36	33	32	27
Sm	5.5	4.2	7.5	5.7	6.4	6.1	5.7	7.4	7.0	7.1	5.1
Eu	1.40	0.92	1.74	1.06	1.40	1.72	1.54	1.32	1.26	2.0	1.14
Gd	4.2	3.4	6.4	4.8	5.6	5.2	4.8	6.0	6.32	5.8	4.0
Tb	0.66	0.60	1.00	0.72	0.84	0.80	0.74	0.94	1.08	0.96	0.60
Dy	3.3	3.1	5.4	4.0	4.6	4.0	3.5	4.8	6.3	4.8	3.1
Ho	0.66	0.66	1.10	0.80	0.98	0.82	0.76	1.02	1.33	1.0	0.64
Er	2.00	1.95	2.90	2.45	2.55	2.25	2.15	2.75	3.96	2.75	1.90
Tm	0.32	0.32	0.44	0.36	0.40	0.36	0.34	0.44	0.61	0.50	0.32
Yb	1.90	2.20	2.70	2.35	2.35	2.20	2.15	2.45	4.0	2.55	1.90
Lu	0.28	0.32	0.30	0.30	0.30	0.32	0.28	0.34	0.56	0.36	0.28
Eu/Eu*	0.90	0.75	0.78	0.63	0.73	0.95	0.92	0.62	0.59	0.97	0.79
(La/Yb) _n	10.8	13.3	8.7	10.7	10.0	11.1	11.21	6.79	3.99	8.5	12.2
NK/A	0.69	0.72	0.68	0.74	0.69	0.73	0.76	0.85	0.68	0.59	0.73
A/CNK	0.98	1.06	1.03	1.1	1.04	0.94	0.95	1.02	1.12	0.99	1.09

4.1. Calc-alkaline suite

Granitoids of this suite are classified as high-K calc-alkaline rocks (Fig. 2). They include monzogranite, granodiorite and quartz monzonite with subordinate syenogranite and quartz monzodiorite (Fig. 3A; Table 2). Agpaitic index (NK)/A for CA rocks (Fig. 3B) does not exceed the upper level of 0.85–0.87 (Liégeois and Black, 1987; Bonin, 2007). In the classification diagram of Sylvester (Fig. 3C) most rock compositions are located in the calc-alkaline field. Although some samples plot

in the field of undivided alkaline and highly fractionated CA granites, all CA rock compositions in this field are situated above the extension of the horizontal line separating the CA and Alk fields. In comparison with the rocks of the alkaline–peralkaline suite, calc-alkaline granitoids are richer in Sr and Ba, but poorer in Zr, Nb (Fig. 4A), K and Y (not shown). Partial overlap in trace element contents of the two suites occurs at silica contents of 74 to 76 wt.%. The most characteristic feature of the CA rocks is higher Eu/Eu* values that vary from 0.5 to 1 and frequently exceed unity (Table 2).

Alkaline, stage 1								Alkaline, stage 2						
		Girgar (16)		Timna (17)		Timna (18)	Yehoshafat(19)		Katharina (20)				Iqna (21)	
S-1724	S-1709	[S-1561]**	S-1569**	217Tm	215Tm	218Tmn	YE10	A37**	D-163**	D-165**	[D-82]	D-43	S-0659	
Gr	Gr	Gr	Gr	Mnz	Mnz	Afs Gr	Afs Gr	Afs Gr	Gr	Gr	Gr	Afs Gr	Gr	
28°03'05"	28°02'51"	28°06'02"	28°07'40"	n.d.	n.d.	n.d.	29°33'27"	29°33'05"	28°36'22"	28°36'01"	28°33'46"	28°32'12"	28°51'49"	
34°17'38"	34°15'35"	34°03'32"	34°02'15"	n.d.	n.d.	n.d.	34°53'54"	34°54'01"	33°56'18"	33°58'09"	33°56'08"	33°51'433"	33°43'21"	
73.5	76.0	73.2	74.0	51.55	52.8	75.3	75.1	74.3	74.0	74.61	75.0	76.8	76.5	
0.31	0.17	0.3	0.28	1.5	1.4	0.16	0.08	0.12	0.2	0.18	0.2	0.07	0.05	
14.15	13.2	14.1	13.9	17.43	14.6	13.02	13.3	13.2	13.2	13.23	12.9	12.1	12.6	
1.6*	0.63	1.6	1.5*	5.65	2.98	1.17	0.89	1.26	1.6*	1.46*	1.5*	1.8*	1.22	
	0.16	0.09		3.23	4.77	0.15	0.38	0.08					0.07	
0.03	0.03	0.06	0.06	0.1	0.13	0.02	0.07	0.14	0.0	0.05	0.1	0.04	0.03	
0.45	0.2	0.3	0.3	4.89	7.4	0.11	0.17	0.18	0.3	0.22	0.2	0.01	-	
1.4	0.8	0.6	0.7	4.69	7.75	0.42	0.38	0.83	0.7	0.74	0.7	0.2	0.4	
3.80	3.40	4.20	4.1	4.36	3.73	3.88	4.72	4.57	3.90	3.81	3.60	3.90	3.90	
4.25	4.60	4.50	4.7	3.41	2.39	5.46	4.32	4.45	5.00	4.95	5.00	4.30	4.20	
0.04	-	-	-	0.77	0.37	0.01	0.04	0.04	0.05	0.05	0.05	0.05	-	
0.45	0.40	0.30	0.2	2.11	1.79	0.51	0.45	0.71	0.50	0.07	0.30	0.30	0.40	
99.98	99.58	99.25	99.74	99.69	100.11	100.21	99.90	99.88	99.49	99.37	99.48	99.57	99.07	
130	120	99	112	85	44	128	105	110	216	243	243	384	253	
173	97	76	88	1200	833	43	40	47	90	86	64.8	5	8	
585	350	368	408	2073	846	401	700	570	309	307	221	42	14	
16	12	22	24	6.1	7.4	14	8	12	19	27	33	71	20	
17.7	14.0	7.4	7.3	3.5	3.4	18.4			26.7	26.0	22.7	36.0	30.6	
7.15	4.35	1.60	1.95	1.28	1.28	3.10			4.50	6.10	5.51	8.60	7.85	
15	10	21	18	8	6	15			21	23	24	43	15	
170	120	340	350	106	153	142	120	130	175	176	184	184	100	
3.2	2.6	1.8	1.8	22.0	4.5	5.4			5.7	5.9	6.3	10.0	3.8	
21	15	51	44	19	23	20	21	19	28	35	41	83	38	
16	14	19	20	23	20	18			19	20	21	28	18	
32	35	28	46	41	39	36	27	29	35	41	32	29	21	
65	70	82	98	76	85	66	52	57.5	79	87	72	68	53	
7	7.0	10.1	14.5				6.3	6.48	8.9	10.4	8.6	8.9	6.6	
27	25	41	57	35	48	25	22	23.06	31	37	31	32	27	
6	4.3	9.4	11.6	7.4	8.9	4.3	3.9	4.04	6.4	7.6	6.6	9.5	7.1	
1	0.68	0.94	1.20	2.16	2.31	0.51	0.26	0.41	0.62	0.67	0.50	0.07	0.01	
4	3.2	8.4	10.1	6.7	7.6	3.7	4.1	3.42	5.0	6.1	5.5	9.8	6.6	
1	0.56	1.50	1.65	0.82	1.00	0.58	0.49	0.52	0.82	1.0	0.92	1.89	1.04	
4	2.9	8.7	9.24				2.7	2.85	4.8	5.9	5.8	12.5	6.2	
1	0.62	1.74	1.81	0.73	1.00	0.86	0.52	0.59	0.92	1.13	1.33	2.79	1.20	
3	1.70	4.82	5.00				1.72	1.76	2.83	3.26	3.63	7.46	3.75	
0	0.28	0.67	0.69	0.24	0.40	0.38	0.28	0.27	0.48	0.63	0.58	1.16	0.50	
3	1.80	4.00	4.17	1.24	2.20	2.50	1.81	1.89	3.22	4.14	3.86	7.48	3.80	
0	0.26	0.48	0.52	0.17	0.28	0.68	0.26	0.29	0.46	0.57	0.57	1.10	0.40	
0.73	0.57	0.33	0.34	0.95	0.87	0.40	0.20	0.34	0.34	0.31	0.26	0.02	0.00	
7.9	13.0	4.7	7.2	21.7	11.6	9.5	9.9	10.1	7.2	6.5	5.4	2.5	3.6	
0.77	0.8	0.84	0.85			0.94	0.94	0.94	0.9	0.88	0.88	0.91	0.87	
1.06	1.1	1.1	1.06			1	1.01	0.95	1.02	1.02	1.02	1.06	1.08	

No significant geochemical distinction is observed between the most abundant granodiorite–quartz monzonite rocks formed at the first (635–615 Ma) and second (610–590 Ma) CA sub-stages. Rocks of both sub-stages contain 63–68 wt.% SiO₂, have similar FeO^t (3–4 wt.%), but variable contents of other elements – (Table 2). CA rocks of the two sub-stages have similar Rb (80–100 ppm) and Ba (600–1000 ppm). However, Nb, Zr, Y, and REE tend to increase and Sr tends to decrease in rocks of the later sub-stage (Figs. 4A and 5A). In granites of the CA suite the difference in chemical composition between rocks of the two sub-

stages is more discernible. The less differentiated granite (Rehavam pluton) representing the early sub-stage is characterized by lower SiO₂ content (73–74 wt.%), Zr (60–70 ppm), Y (6–12 ppm), Nb (6–12 ppm) and enhanced Sr (340–450 ppm), as compared with granite from the later sub-stage (Fig. 4A). Also characteristic is low REE content and poorly exhibited negative Eu anomaly (Fig. 5B, Table 2). In all granites of the second sub-stage a negative Eu anomaly is pronounced (the average Eu/Eu* value is 0.68) and concentrations and patterns of REE are similar (Fig. 5B).

Table 2 (continued)

Suite	Alkaline, stage 2											
Pluton/Complex	Iqna (21)	Umm Shomer (22)		Dahab (23)		Sahara (24)			Sharm (25)			Serbal (26)
Sample no.	S-0782	[S-1885]	S-1883	S-3968	[S-3896]	S-1600**	S-1496	[S-1542]	S-1529**	S-1384**	[S-1518]	S-0815
Rock type	Gr	PA Gr	Afs Gr	Gr	Gr	PA Gr	PA Gr	PA Gr	Afs Gr	Afs Gr	Q-Afs Sy	PA Gr
Latitude N	28°48'59"	28°21'51"	28°21'41"	28°35'26"	28°22'08"	28°01'43"	27°58'21"	28°09'19"	27°57'50"	27°51'44"	27°54'27"	28°39'02"
Longitude E	33°45'57"	33°55'18"	33°55'01"	34°24'00"	34°24'38"	34°09'39"	34°05'46"	33°59'05"	34°16'33"	34°16'04"	34°11'15"	33°48'36"
SiO ₂	77.7	76.3	73.7	70.6	69.50	74.72	75.49	77.5	69.76	73.61	67.13	76.4
TiO ₂	0.09	0.18	0.19	0.53	0.55	0.18	0.38	0.16	0.41	0.19	0.55	0.05
Al ₂ O ₃	12.5	12.5	14	13.4	14.40	11.38	11.23	11.1	13.85	12.97	13.5	12.6
Fe ₂ O ₃	1.23	1.4*	1.0*	2.32	1.80	1.56	0.95	1.5*	1.61	1.78	2.30	1.3*
FeO	0.25			1.58	1.60	0.89	1.45		2.25	0.41	2.89	
MnO	0.04	0.07	0.06	0.09	0.07	0.06	0.07	0.05	0.09	0.06	0.17	0.02
MgO	0.1	0.1	0.2	0.4	0.60	0.07	0.09	0.05	0.44	0.15	0.30	0.05
CaO	0.6	0.4	0.6	1.3	1.60	0.46	0.27	0.3	1.23	0.42	1.10	0.4
Na ₂ O	3.90	4.50	4.60	3.90	3.90	4.34	3.73	3.50	4.54	3.78	4.75	4.90
K ₂ O	4.20	5.10	5.20	5.00	5.00	5.03	5.54	4.80	5.42	5.64	5.58	4.70
P ₂ O ₅	-	-	-	0.1	0.10	0.01	0.01	0.05	0.09	0.02	0.06	0.05
LOI	0.40	0.10	0.30	0.20	0.20	0.45	0.55	0.30	0.35	0.86	1.38	0.30
Total	100.20	100.65	99.85	99.42	99.32	99.15	99.76	99.71	100.04	99.89	100.3	100.60
Rb	228	180	135	120	110	160	151	140	95	158	117	202
Sr	12	17	57	100	80	11	12	11	88	48	38	4
Ba	41	135	332	301	560	37	8	bdl	400	265	370	8
Nb	17	20	15	52	39	36	24	13	40	29	56	24
Th	33.8	14.9	12.7	13.8	13.6	17.3	12.6	9.1	14.1	22.0	8.5	22.4
U	9.65	3.20	2.25	2.75	3.15	6.35	2.95	2.85	3.05	5.0	2.6	8.10
Pb	25	30	29			25	20	20	19	23	16	20
Zr	200	230	180	700	500	316	700	870				210
Hf	5.6	4.6	3.2	3.6	3.4	9.2	4.8	6.4	3.2	4.2	1.4	8.4
Y	41	31	24	52	46	46	40	34	67	51	49	53
Ga	17	16	16	29	29	25	23	23	25	24	26	22
La	29	35	45	89	58	34	93	110	98	93	38	22
Ce	68	77	88	190	190	75	200	190	205	189	100	63
Pr	8.9	8.8	9.4	22.6	14.6	10.5	22.0	24.9	29	25.8	12.7	9.5
Nd	35	34	34	85	53	42	78	87	114	97	53	41
Sm	7.7	7.1	6.4	14.8	14.3	8.8	12.8	13.8	21.04	15.85	12.1	11.6
Eu	0.10	0.72	0.96	1.50	1.36	0.45	0.66	0.58	1.84	1.3	2.02	0.06
Gd	5.8	6.6	5.4	13.0	11.0	7.5	11.0	11.0	18.35	13.5	12.0	11.0
Tb	1.04	1.08	0.86	2.00	1.74	1.23	1.52	1.44	2.76	1.84	1.76	1.80
Dy	5.4	5.9	4.5	9.9	8.9	6.9	7.8	6.3	14.41	9.5	9.9	9.8
Ho	1.12	1.20	0.94	1.92	1.32	1.39	1.80	1.12	2.8	1.87	1.90	1.96
Er	3.25	3.50	2.65	5.55	4.90	4.07	4.40	3.65	7.67	5.39	6.0	5.15
Tm	0.52	0.52	0.42	0.80	0.72	0.63	0.58	0.48	1.05	0.78	0.82	0.78
Yb	3.25	3.30	2.50	5.00	4.50	4.32	3.95	3.35	7.05	5.16	5.45	4.65
Lu	0.48	0.48	0.36	0.68	0.52	0.66	0.54	0.44	1.08	0.78	0.78	0.64
Eu/Eu*	0.05	0.33	0.51	0.33	0.33	0.17	0.17	0.15	0.29	0.28	0.52	0.02
(La/Yb) _n	5.9	7.1	11.9	11.8	8.5	5.2	15.6	21.7	9.2	11.9	4.6	3.1
NK/A	0.88	1.03	0.94	0.88	0.82	1.11	1.08	1.04	0.89	0.95	1.03	1.04
A/CNK	1.04	0.92	0.98	0.94	0.98	0.85	0.89	0.91	3.43	0.99	0.85	0.91

4.2. Alkaline–peralkaline granite suite

Three main rock types, syenogranite, Afs and PA granite, are recognized in the suite (Fig. 3A). Most Alk granites are characterized by agpaite index (NK)/A ranging from 0.8 to 1.1 (Fig. 3B). Lower values, 0.8–0.85, are observed only in few syenogranite samples. On Sylvester's diagram (Fig. 3C) the rock compositions plot in the "Alkaline granite" field and in the lower part of the undivided field, mostly below the extension of the horizontal borderline. Unlike CA granites, all rock types of the Alk suite have low Eu/Eu* < 0.5 and

include high silica varieties with SiO₂ > 76 wt.% (Table 2; Fig. 4A). Alk granites plot within the A-type granite field in classification diagrams (Fig. 6) with one exception of granite from the Umm-Shomer pluton caused by anomalously low Ga content of 16–17 ppm (Table S1).

Chemical compositions of Alk granite from the early sub-stage (>600 Ma) plot in the border zones between Alk and CA granites in various discrimination diagrams (Figs. 3B and 4A). Nevertheless, in most diagrams they are confined to the alkaline fields. This is also clearly exhibited in a set of silica variation diagrams in the Supplementary data (Figs. 3A-SD and 3B-SD). The composition of

		Umm-Ifai (27)				Bimodal dyke suite (28)				International standards				
S-0824	S-0826	S-4519	S-4546**	S-4543**	[S-4403]	N-1b**	A196-1	A-128	A66-3b**	SO-3	NIM-G			
Afs Gr	Gr	Gr	Gr	Gr	Afs Gr	Tdol	Tdol	QP	QP		Lab-1	Lab-1	Lab-2	
28°36'44"	28°36'21"	28°44'01"	28°43'33"	28°42'13"	28°43'38"	29°35'38"	29°35'38"	29°33'40"	29°31'25"					
33°38'25"	33°37'08"	34°36'17"	34°37'08"	34°36'01"	34°34'58"	34°35'47"	34°35'47"	34°54'08"	34°55'28"					
75.5	73.8	72.2	71.8	73.4	77.8	52.8	50.8	77.0	76.2	33.7	33.1	75.7	75.6	75.9
0.05	0.2	0.3	0.3	0.2	0.1	1.72	1.83	0.1	0.1	0.33	0.34	0.09	0.1	0.08
12.5	13.6	13.8	14.2	13.5	11.6	14.7	15.3	11.9	11.6	5.8	5.85	12.08	11.59	12
1.7*	2.1*	2.6*	3.0*	2.8*	1.3*	4.82	3.44	1.7	2.7	2.22	2.18	2.02	2.06	1.09
						4.1	4.35	0.2	0.2					0.95
0.02	0.02	0.06	0.06	0.05	0.02	0.18	0.17	0.0	0.0	0.07	0.07	0.02	0.03	0.02
0.05	0.2	-	-	-	-	4.6	4.47	0.3	0.1	8.42	8.49	0.06	0.06	0.07
0.5	0.9	1.10	1.0	0.9	0.1	6.0	6.28	0.5	0.2	20.7	20.85	0.78	0.8	0.81
4.30	4.00	4.30	4.20	3.90	4.00	3.27	3.79	3.90	3.00	1.01	1.00	3.36	3.41	3.29
4.50	5.00	5.10	4.80	4.70	4.30	2.76	3.20	4.08	5.40	1.40	1.44	4.99	5.05	5.00
0.05	0.05	0.1	0.1	0.1	0.09	0.4	0.38	0.01	-	0.1	0.08	0	0	0
0.20	0.40	0.40	0.40	0.90	0.30	4.65	5.44	0.56	0.82					
99.20	100.27	99.96	99.86	100.45	99.61	100.00	99.45	100.13	100.40					
125	107	160	140	150	150	65	86	140	194	39				
11	75	102	103	97	5	430	460	13	60	222				
75	27	390	403	361	16	750	940	70	150	290				
17	14	57	52	37	110	18	13	29	34	6.4				
14.4	10.9	20.1	16.1	16.3	14.0	3.7	4.2	15.4	17.7	3.9				
4.10	2.75	4.85	3.90	5.70	5.05	0.81	1.15	4.14	5.75	1.10				
10	10	35		30	4	9	11	8	65					
310	330	400	440	330	390	220	210	600	590					
6.6	4.0	5.0	4.6	5.4	8.8	4.7	5.2	13.3	14.4					
42	22	39	34	32	62	26	28	78	75	24.5	26.6			
21	18	30	27	28	36	20	23	20	19					
28	55	80	60	48	62	28	24	29	43	17	17			
84	110	170	115	91	130	58	52	69	102	34	36			
12.6	12.6	17.9	14.4	11.7	18.4	6.8	7.1	8.7	12.2	4.6	4.8			
56	46	60	53	43	72	28	30	35	50	17	15			
14.2	8.0	11.1	10.0	8.3	18.0	5.6	6.1	8.8	11.6	3.5	3.6			
0.14	0.60	1.22	1.27	1.04	0.52	1.58	1.50	0.14	0.28	0.70	0.74			
13.0	5.8	9.2	8.9	7.2	17.0	5.2	6.4	8.8	11.0	3.1	3.2			
1.98	0.90	1.52	1.43	1.14	2.76	0.81	0.80	1.53	1.93	0.48	0.49			
9.8	4.4	8.8	8.0	6.4	16.1	4.7	4.2	9.8	11.2	2.8	3.0			
1.88	0.86	1.66	1.66	1.35	3.14	0.94	0.80	2.18	2.33	0.60	0.64			
4.50	2.45	5.20	4.85	4.08	8.70	2.60	2.35	6.01	6.73	1.90	1.84			
0.60	0.34	0.86	0.74	0.63	1.22	0.37	0.33	0.90	1.02	0.24	0.22			
3.40	2.15	5.60	4.86	4.41	7.15	2.45	1.96	5.65	6.57	1.70	1.75			
0.48	0.32	0.78	0.73	0.69	1.00	0.37	0.29	0.83	0.98	0.23	0.23			
0.03	0.27	0.37	0.42	0.42	0.09	0.89	0.74	0.05	0.08					
5.5	16.9	9.4	8.2	7.2	5.7	7.6	8.1	3.4	4.4					
0.96	0.88	0.91	0.85	0.85	0.97			0.91	0.93					
0.97	1	0.95	1.02	1.03	1.02			1.01	1.04					

syenogranite from the later sub-stage (600–580 Ma) varies in different plutons. Selected silica variation diagrams (Fig. 7) demonstrate compositional distinctions of syenogranites from four plutons wherein syenogranite is dominant (Tables 2 and 1-SD). Though each individual pluton is more or less homogenous (except of the Dahab pluton incorporating varieties with evidence of hybridization, see Table 1), taken together they cover the whole silica range of granite, from 69 to 78 wt.% SiO₂. Large silica variations are accompanied by significant variations in several major and trace element contents, most prominently in Sr, Ba, Zr, Rb (Fig. 7) and CaO (not shown).

Afs and PA granites are richer in alkalis and Zr compared to syenogranite with the same silica content (Fig. 7). These two granite types are similar in major and trace element contents; the exception is higher concentrations of Rb and Nb mostly in the Afs granite from the Katharina pluton (Fig. 7; Table 2). Overall, the only conspicuous difference between Afs and PA granites is slightly higher value, up to 1.1, of the agpaic index in the latter (Fig. 3B).

Despite the great diversity in REE patterns observed in granites from the alkaline–peralkaline suite, overall these rocks are noticeably distinguished from the CA granitoids by higher ΣREE and much lower

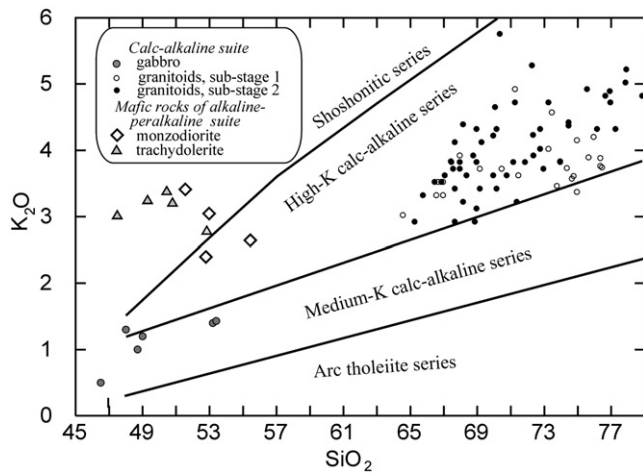


Fig. 2. SiO_2 vs. K_2O classification diagram with the boundary lines after Le Maitre (1989) and Rickwood (1989).

Eu/Eu^* values (Fig. 4B; Tables 2 and 1-SD). REE patterns overlap only in a fairly narrow field and CA and Alk granites in this field have distinct negative Eu anomalies. Compositions of Afs quartz porphyry from the bimodal dike suite that is abundant in southern Israel (Table 1) are very similar to Afs granite (Tables 2 and 1-SD).

The main distinctive geochemical features of granitoids from the CA and Alk suites are summarized in Table 3.

Mafic rocks occur in both igneous suites (see above). In the CA suite, gabbro and diorite were emplaced at ~630 Ma (Table 1). Mafic rocks from the Alk suite are confined to the Timna monzodiorite (sub-stage 1) and to trachydolerite from the bimodal dyke suite (later sub-stage, ~595 Ma). They are characterized on the basis of previously published data (Beyth et al., 1994; Katzir et al., 2007a,b). Typical chemical data are given in Table 2.

The chemical compositions of mafic rocks from the CA and Alk suites are significantly different. Rocks from the CA suite plot in the calc-alkaline field in conventional classification diagrams (not shown). In the SiO_2 vs. K_2O diagram (Fig. 2), gabbro is referred to as medium-K calc-alkaline, whereas monzodiorite and trachydolerite plot mostly in the shoshonite field with high $\text{K}_2\text{O} = 2.5\text{--}3$ wt.%. Calc-alkaline gabbro has high alumina ($\text{Al}_2\text{O}_3 = 16.6\text{--}19$ wt.%), moderate Mg numbers ($\text{Mg}\# = 49\text{--}60$), and enhanced CaO (7.7–11 wt.%). By contrast Alk mafic rocks have low alumina ($\text{Al}_2\text{O}_3 = 14.11\text{--}15.8$ wt.%), low-to-moderate Mg numbers (50–70 in monzodiorite and 40–55 in trachydolerite), and moderate CaO from 5 to 7 wt.%. The concentrations of some trace elements in the two suites are also different, as shown by the enhanced Sr (620–900 ppm) and low Ba (210–460 ppm), Zr (40–85 ppm), Y (10–20 ppm), Nb (4–8 ppm) and $\Sigma\text{REE} = 92$ ppm (average) in the CA gabbros. The $(\text{La}/\text{Yb})_n$ ratios range from 4 to 8, and Eu/Eu^* ratios are close to unity (Fig. 5C). By contrast, mafic rocks from the Alk suite contain much higher Ba (800–1200 ppm) and Zr (100–180 ppm in monzodiorite and 210–320 ppm in trachydolerite). Trachydolerite, as compared with monzodiorite, is richer not only in Zr, but also in Nb. The contents of REE in Alk mafic rocks (140–195 ppm) are noticeably higher than those of CA gabbro (50–130 ppm), though REE patterns are similar in shape and slope (Fig. 5C).

5. Rb–Sr and Sm–Nd isotope characteristics

Sr–Nd isotope data for 26 representative samples are given in Table 4. Initial $^{87}\text{Sr}/^{86}\text{Sr}$ ratios, or $I(\text{Sr})$ values, for 14 rocks with “low” $^{87}\text{Rb}/^{86}\text{Sr}$ ratios (≤ 1) show a rather limited range from 0.7028 to 0.7048 except for one case (N-1, trachydolerite dyke). This is comparable to the $I(\text{Sr})$ of the hypothetical primitive mantle source

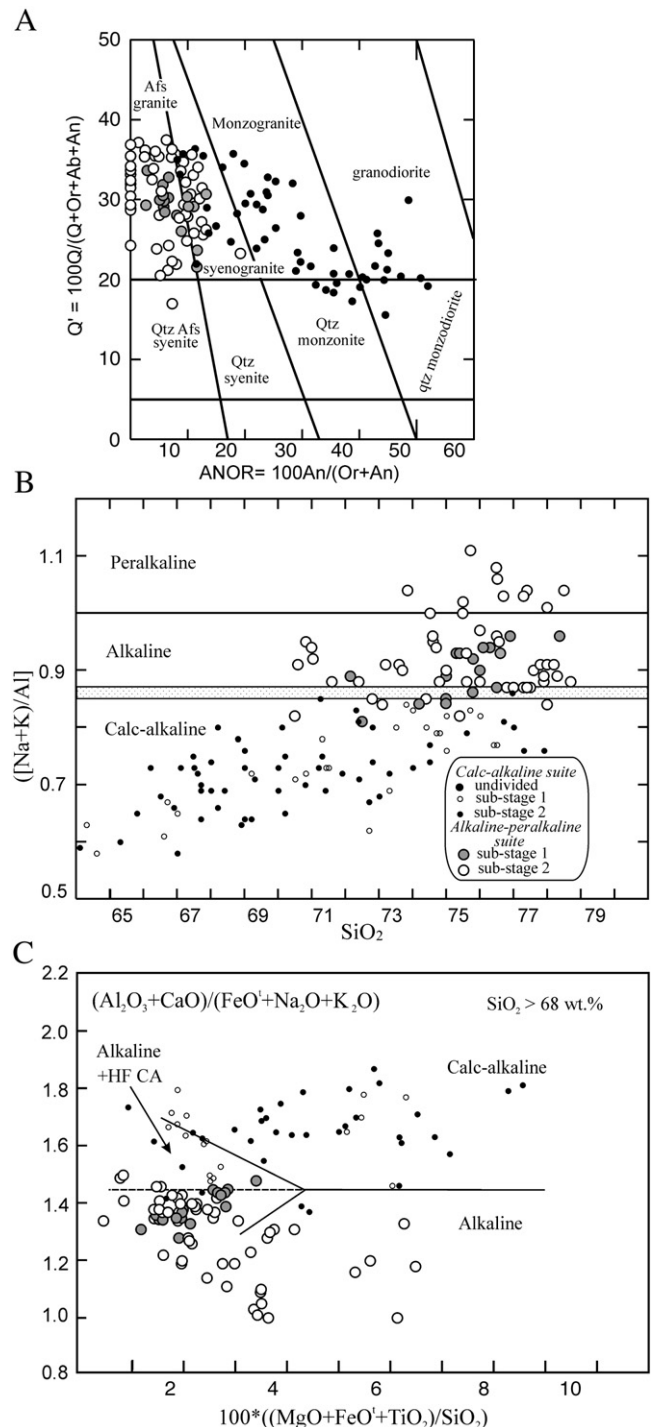


Fig. 3. Compositions of granitoids from the CA and Alk suites in selected classification diagrams. A, $100\text{An}/(\text{Or} + \text{An})$ vs. $100\text{Q}/(\text{Q} + \text{Or} + \text{Ab} + \text{An})$ diagram, after Streckeisen and Le Maitre (1979). B, SiO_2 vs. NK/A (agpaite index, mol%), after Liégeois and Black (1987). C, $100 * ((\text{MgO} + \text{FeO} + \text{TiO}_2)/\text{SiO}_2)$ vs. $(\text{Al}_2\text{O}_3 + \text{CaO})/(\text{FeO} + \text{Na}_2\text{O} + \text{K}_2\text{O})$, after Sylvester (1989). HF CA = high fractionated calc-alkaline granite.

(ca. 0.7042). Note that rocks with high or very high Rb/Sr ratios could not yield precise and meaningful $I(\text{Sr})$ values due to the large correction for radiogenic ^{87}Sr . Consequently, the calculated $I(\text{Sr})$ values for these rocks are not used for petrogenetic discussion. Indeed Table 4 shows some aberrant $I(\text{Sr})$ values obtained for high Rb/Sr rocks such as three Alk granites (A-37, S-1600, S-1384) and one rhyolite (147–2) that have anomalously high ratios from 0.7150 to 0.7433; likewise three other Alk granites (MB-115, D163, D165) give unreasonably low ratios of 0.6954 to 0.7002. High $I(\text{Sr})$ values may

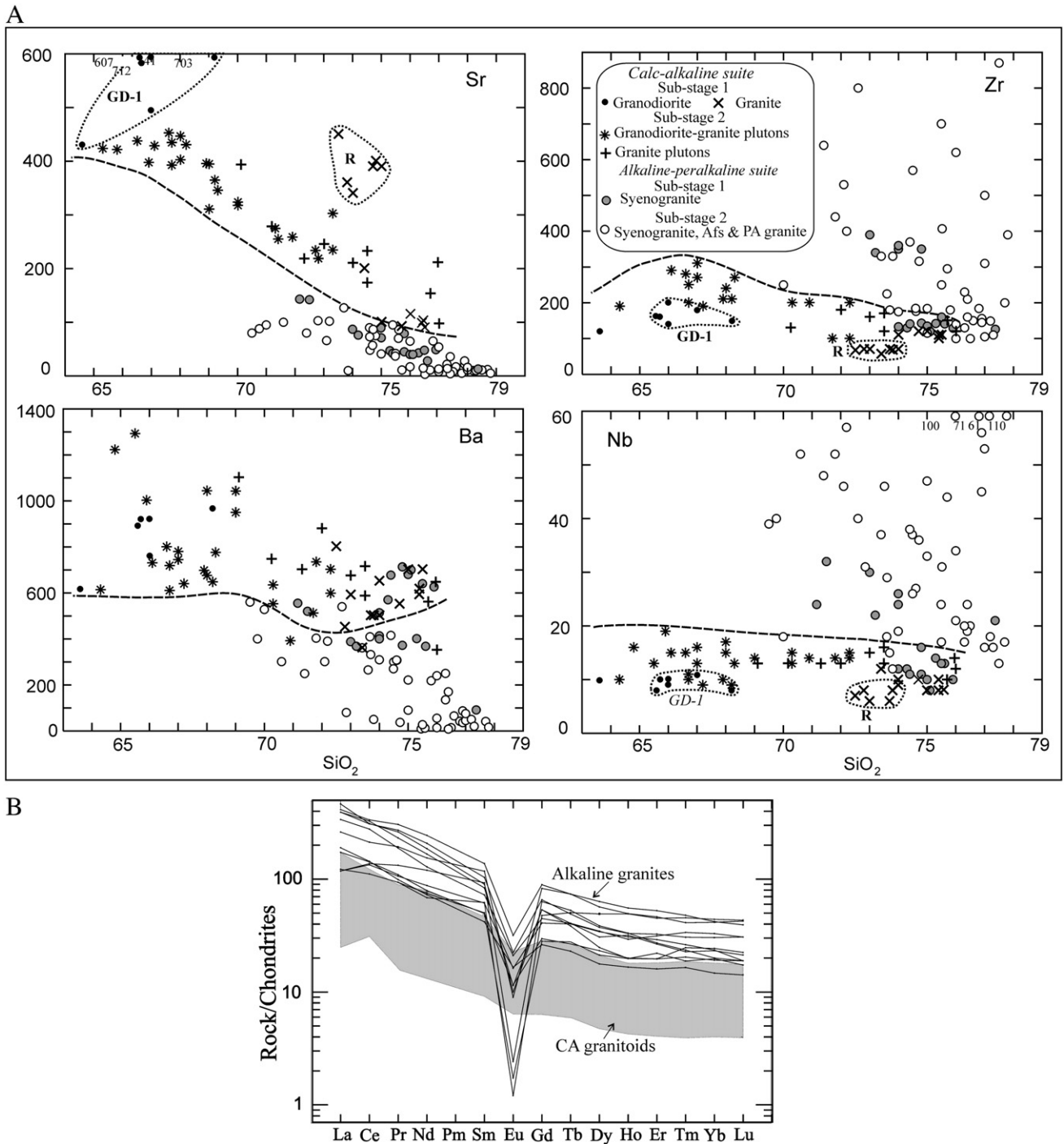


Fig. 4. A, silica variation diagrams demonstrating distinctions between the granitoids from the CA and Alk suites and compositional variations within the suites. B, REE patterns for granitoids from the CA and Alk suites. Abbreviations: Afs = alkali feldspar; PA = peralkaline; GD-1 = compositions of CA granodiorite from the early sub-stage; R = Rehavam pluton. In this and other figures, the term ‘granodiorite’ includes also quartz monzonite and quartz monzodiorite.

have resulted from post-magmatic disturbance of the Rb–Sr isotopic system, including modification of Rb/Sr ratios and enhancement of ⁸⁷Sr/⁸⁶Sr ratios by high ⁸⁷Sr/⁸⁶Sr contaminant (rock or fluid). Positive correlation of Sr and oxygen isotope ratios in Late Neoproterozoic granites and dyke rocks of Sinai and southern Israel (Katzir et al., 2007b) indicated that the enhanced I(Sr) values in whole-rock samples were the result of extensive low-temperature alteration. The water–rock interaction had significantly elevated both the oxygen and Sr isotope ratios in feldspar-dominated rocks. However, nearly initial magmatic δ¹⁸O values are preserved even in feldspar minerals

in several locations including the Katharina ring complex, Rehavam granite and Timna complex (Table 7 in Katzir et al., 2007b).

The Sm–Nd isotope system appears to be unaffected by the low-temperature alteration (Katzir et al., 2007b). All ε_{Nd(T)} values are positive regardless of the rock type and affiliation to a certain rock suite. They range from +2.4 to +4.7 in the CA suite and from +2.5 to +5.5 in the Alk suite (Table 3; Fig. 8A and B). Taking into account the error limits (±0.5), the two suites cannot be distinguished isotopically. The two-stage model ages (Nd TDM) vary from ca. 860 to 1200 Ma for the CA suite, and from ca. 800 to 1100 Ma for

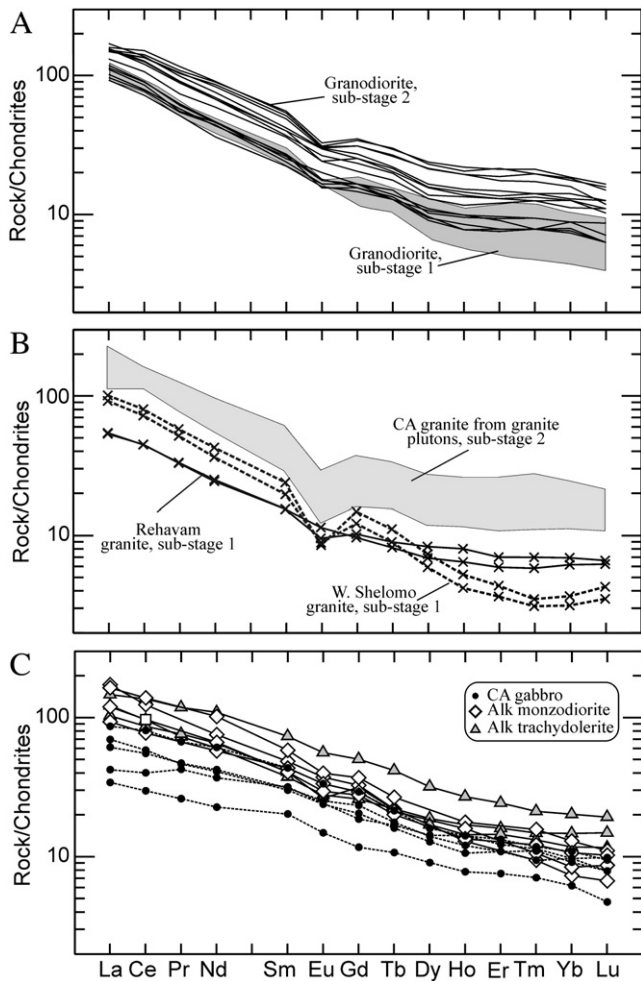


Fig. 5. REE patterns in CA granitoids and selected mafic rocks. A, first and second sub-stages of CA granodiorite, quartz monzonite. B, CA granites of two sub-stages; the first (crosses) includes less differentiated granite from the Rehavam pluton and highly differentiated granite from the Nahal Shelomo pluton; gray field incorporates granites from the second sub-stage. C, REE patterns of CA gabbro and mafic rocks from the Alk suite. Here and in Figs. 10 and 12 chondrite values are after Sun and McDonough (1989).

the Alk suite. The single-stage model ages are quite similar to the two-stage model ages, suggesting that $f(\text{Sm}/\text{Nd})$ values for most rocks are close to that of the average continental crust (-0.4 to -0.6).

6. Discussion

6.1. Origin of mafic and silicic magmas

6.1.1. Evidence from Sr–Nd and oxygen isotope ratios

Radiogenic isotope ratios are commonly considered as the most reliable tracers of magma sources. However, in regions dominated by young juvenile crust, like the ANS, the petrogenetic significance of the isotope data can be ambiguous (Stern, 2002; Hargrove et al., 2006; Liégeois and Stern, 2009). In the following petrogenetic discussion, we use all the available Sm–Nd isotope data, including our new data reported herein and the literature data of ~120 samples of igneous and metamorphic rocks from southern Israel, southwestern Jordan, Sinai Peninsula and Eastern Desert, Egypt (Table 4 and Table 2-SD, Supplementary data).

The indistinguishable $\varepsilon_{\text{Nd}(T)}$ values of felsic and mafic rocks shown in Fig. 8C may suggest a genetic link between them and derivation of both felsic and mafic magmas from a common source. However, some of the older metaigneous rocks that formed in the island arc stage at

700–850 Ma have higher $\varepsilon_{\text{Nd}(700-850 \text{ Ma})}$ from +4 to +8 (Fig. 8C). One to two hundred million years after their formation, during the post-collisional stage, the $\varepsilon_{\text{Nd}(580-630 \text{ Ma})}$ values of the island arc rocks had decreased and ranged from +1 to +6 (Fig. 8C), which overlaps the $\varepsilon_{\text{Nd}(T)}$ values of CA and Alk rocks. It follows that the $\varepsilon_{\text{Nd}(T)}$ values of the post-collisional granitoids could have been acquired either by partial melting of older island arc juvenile crust or by fractional crystallization of mantle-derived parental mafic magma at about 600 Ma. The Nd model ages of the island arc and post-collisional Neoproterozoic rocks from the northern ANS are similar, from ca. 800 to 1300 Ma (Table 4 and Table 2-SD), suggesting little or no Archean or early Proterozoic rocks existing in the lower to middle crust of the northern ANS. This inference is supported by the U–Pb dating of individual zircon grains from various plutonic rocks from the Sinai Peninsula (Be’eri-Shlevin et al., 2009a) and by radiogenic isotope studies of whole-rock samples of Neoproterozoic granite–gneiss in the Eastern Desert, Egypt (Liégeois and Stern, 2009).

Three models for the generation of the CA and Alk silicic magma should thus be considered as equally probable: (1) partial melting of the young juvenile crust that formed at the island arc and collisional stages; (2) fractional crystallization of mantle-derived mafic magma at post-collisional stage, or partial melting of slightly older mafic rocks; and (3) mixing of mafic and juvenile crust-derived silicic magmas followed by fractional crystallization of the hybrid melts.

Oxygen isotope ratios of rocks and minerals are very sensitive to low-temperature interaction with the hydrosphere and thus, unlike radiogenic isotope ratios, $\delta^{18}\text{O}$ makes an excellent indicator for recycling of supracrustal material even when juvenile crust is involved. Oxygen isotope ratio of zircon [$\delta^{18}\text{O}(\text{Zrn})$] has been shown to preserve the original magmatic $\delta^{18}\text{O}$ even through hydrothermal alteration and high temperature metamorphism (Valley, 2003). The asthenospheric mantle is a fairly homogenous oxygen isotope reservoir (Eiler, 2001), and igneous zircons in high temperature equilibrium with mantle-derived magma have an average $\delta^{18}\text{O}(\text{Zrn}) = 5.3 \pm 0.6\%$ (2σ ; Valley et al., 1998). Significant deviation of $\delta^{18}\text{O}(\text{Zrn})$ from the mantle value is commonly interpreted to result from interaction of magma with upper crustal materials either by subduction or assimilation. Be’eri-Shlevin et al. (2009b) measured oxygen isotope ratios in bulk zircon separates of ca. 40 plutons of southern Israel and Sinai. The full dataset and interpretation are given in the cited paper. In summary, $\delta^{18}\text{O}(\text{Zrn})$ values of the CA and Alk suite rocks range from 5.1 to 7.1‰ and 4.5 to 8.0‰, respectively. Normalization using the surface exposure of each sampled rock unit yielded indistinguishable average $\delta^{18}\text{O}(\text{Zrn})$ values: 5.7‰ for the CA and 5.8‰ for the Alk suite. This indicates that both the CA and Alk magmatic suites are derived from sources with mantle-like $\delta^{18}\text{O}$ values. A possible contribution from upper crustal sources is suggested in a small proportion of igneous rocks. Oxygen isotope ratios, like radiogenic isotope ones, cannot easily distinguish the mantle from the juvenile lower crust contributions to magmas. Thus the origin of post-collisional magmas should be further constrained by their trace element compositions.

6.1.2. Geochemical evidence

Fig. 9 shows two sets of MORB-normalized spidergrams, one for mafic and the other for felsic rocks. The average compositions of mafic rocks from the two suites are compared: CA gabbro ($630 \pm 4 \text{ Ma}$), and Alk monzodiorite from the Timna Complex ($602 \pm 5 \text{ Ma}$) and trachydolerite from the bimodal dyke suite ($\sim 595 \text{ Ma}$). All three rock types contain 50–52 wt.% SiO_2 . The CA gabbro is enriched in LILE (K, Rb, Ba, Th) and shows clear negative Nb anomaly, which is typical of subduction zone calc-alkaline rocks. The slightly positive $\varepsilon_{\text{Nd}(T)}$ values for CA mafic rocks (+2 to +4.5; Fig. 8) suggest that the source was probably depleted lithospheric mantle with some subducted crustal component.

Mafic rocks from the Alk suite are clearly distinguished from the CA gabbro by much higher contents of LILE, as well as by higher Nb, Zr,

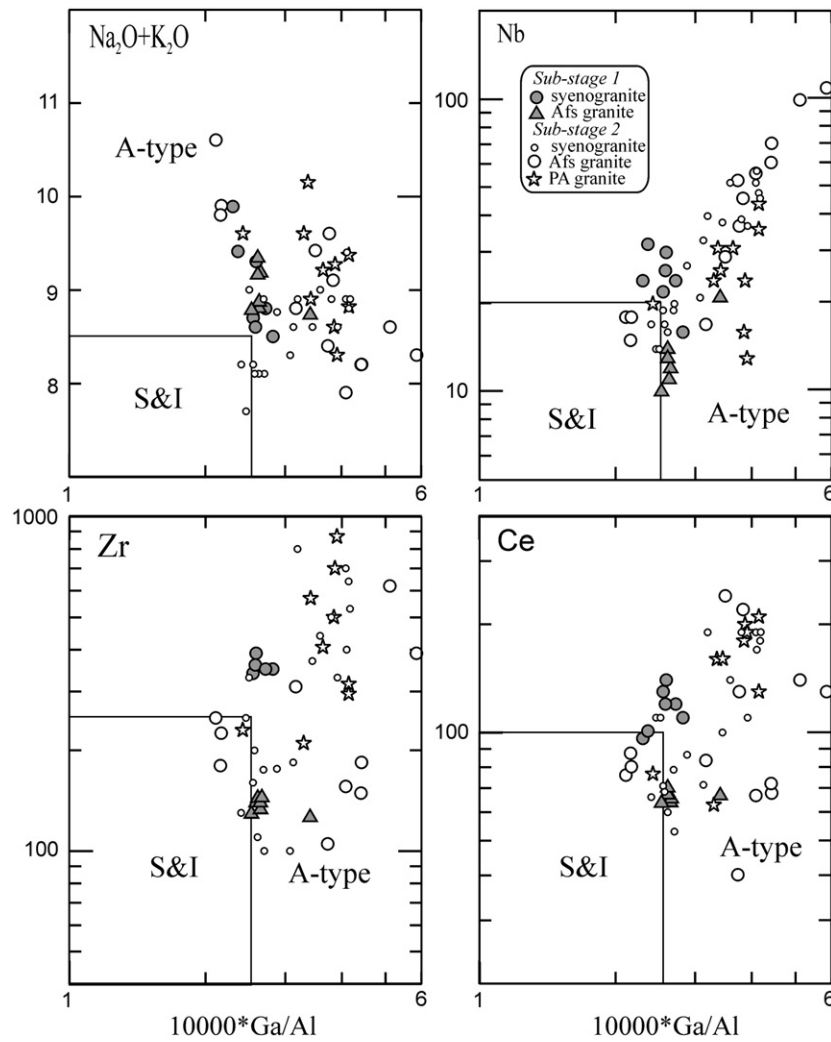


Fig. 6. $10,000 \cdot \text{Ga}/\text{Al}$ vs. $(\text{Na}_2\text{O} + \text{K}_2\text{O})$, Nb, Zr and Ce classification diagrams, after Whalen et al. (1987).

Y, P, Ti (in trachydolerite) and LREE (Figs. 9A and 5C). This calls for either a different mantle source for the Alk mafic rocks or enrichment of the existent (CA) mantle source by incompatible elements prior to the magma generation. HFSE patterns of the monzodiorite and trachydolerite resemble those of OIB (Fig. 9A), though they are richer in LILE and, unlike OIB, retain negative Nb anomaly that decreases from the older monzodiorite to younger trachydolerite. Overall, similarity to OIB and high-Ti and high-P abundances suggests derivation of the Alk basic magma from enriched mantle sources. Enriched mantle (EM-I and EM-II) is, however, characterized by negative $\varepsilon_{\text{Nd}(T)}$ values (Zindler and Hart, 1986), whereas in all mafic rocks from the Alk suite $\varepsilon_{\text{Nd}(T)}$ values are positive (Fig. 8). This suggests that the Alk mafic rocks were not derived from a long-lived enriched mantle sources like EM-I or EM-II. The range of $\varepsilon_{\text{Nd}(T)}$ in the mafic Alk rocks, from +1.5 to +5, and the subdued Nb anomaly (Fig. 9A) suggest that the source region was situated in the moderately depleted lithospheric mantle that was enriched to various extents in LILE and HFSE by the influx of magmatic melts/fluids from the asthenospheric mantle. The enrichment of the trachydolerite and monzodiorite in K and Rb, as well as in REE and other HFSE (Tables 2 and 1-SD) can be related to an asthenospheric effect combined with melting of the metasomatized lithospheric mantle wedge itself (Stein et al., 1997).

The trace element patterns of felsic rocks shown in Fig. 9B represent three felsic rock types: (i) the average contents of CA granite from the granodiorite–granite plutons, (ii) the least differen-

tiated Alk syenogranite from the Umm-Ifai pluton (see below Fig. 11 and comments in the text), and (iii) the quartz porphyry coeval with trachydolerite in the bimodal dyke suite (Katzir et al., 2007b). The temporal increase in K, Rb, Zr and REE contents that characterizes the mafic rocks is also evident in granites. The lower Sr, Ba, Ti and P contents in granites relative to the coeval mafic rocks can be simply the result of the fractionation process that is inherent from the granite magma genesis. In either case, the important geochemical distinctions between mafic rocks from CA and Alk suites are also evident in the felsic rocks (Fig. 9A and B), thus suggesting that the trace element characteristics of the CA and Alk granites were mostly inherited from parental mantle-derived mafic material. Hence it follows that the generation of silicic magma solely by melting of metamorphic crustal source is unlikely. Nonetheless significant crustal contribution to magmas of some CA granite plutons from southern Israel, Sinai (Eyal et al., 2004; Be'eri-Shlevin et al., 2009b) and the Eastern Desert, Egypt (El-Sayed and El-Nisr, 1999; Moghazi, 1999; El-Nisr et al., 2001) should be considered.

6.2. Genetic interrelations between various granite types in the CA and Alk suites

6.2.1. Calc-alkaline suite

The calc-alkaline suite comprises a continuous compositional sequence from gabbro to diorite to granodiorite (\pm quartz monzonite) and granite. Two important geochemical and textural features

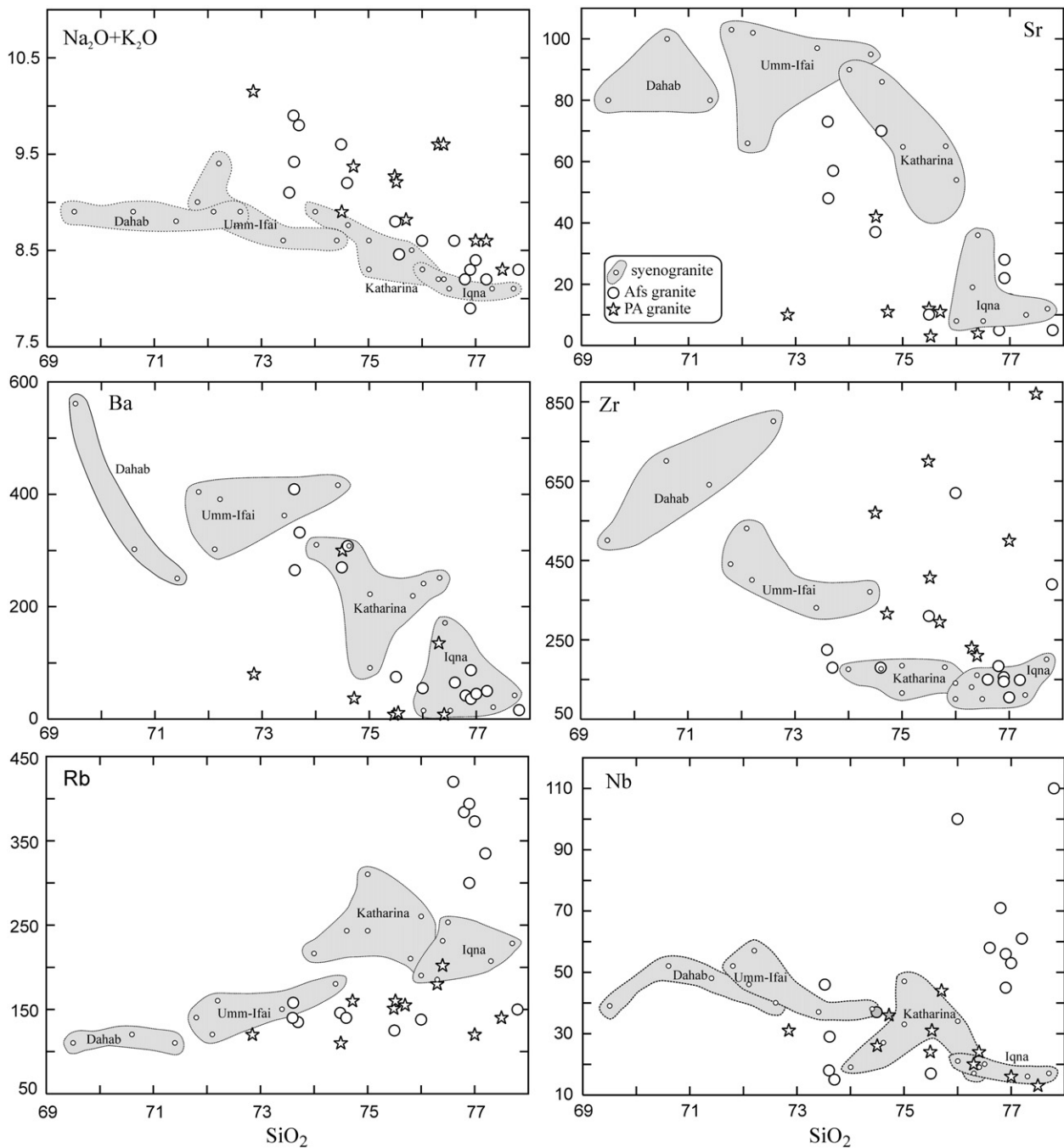


Fig. 7. Silica variation diagrams for Alk granites (stage 2) showing significant range of the syenogranite compositions and overlap of the Afs and PA granite compositions.

Table 3
Geochemical distinctions between granitoids from CA and Alk suites.

Distinctive features	CA granitoids	Alk granitoids
Rock types; underlined are dominant types, see Fig. 5A and Table 1	<u>Monzogranite</u> <u>Granodiorite</u> Syenogranite Qtz monzonite Qtz monzodiorite	<u>Syenogranite</u> <u>Afs granite</u> Peralk. granite
Agpaitic index (Na + K)/Al, see Fig 5B	<0.85–0.87; ranges from 0.58 to 0.87	Mostly > 0.85; ranges from 0.8 to 1.1
Ratio K ₂ O/Na ₂ O, see Tables 2 and 1-SD	<1 in 90% of samples	> 1 (except the Yehoshafat pluton)
Ratio (Al ₂ O ₃ + CaO)/(FeOt + Na ₂ O + K ₂ O), see Fig. 5C	1.40–1.85 (except two samples)	0.97–1.50
Selected trace elements in rocks with similar SiO ₂ content, see Fig. 6, Table 2	Higher Sr, Ba	Higher Zr, Nb, Y
Σ REE	50–190 ppm	140–450 ppm
Eu/Eu*, see Tables 2 and 1-SD	Mostly >0.5; values > 1 are common	<0.5, commonly <0.4

Table 4
Rb–Sr and Sm–Nd isotope data of plutonic rocks from the Sinai Peninsula and S. Israel.

Pluton	Sample number	Rock type, SiO ₂ , wt.%	Age (Ma)	Rb (ppm)	Sr (ppm)	⁸⁷ Rb/ ⁸⁶ Sr	⁸⁷ Sr/ ⁸⁶ Sr	±2σ	I(Sr)	Sm (ppm)	Nd (ppm)	¹⁴⁷ Sm/ ¹⁴⁴ Nd	¹⁴³ Nd/ ¹⁴⁴ Nd	±2σ	ε _{Nd(t)}	f (Sm/Nd)	ε _{Nd(T)}	T _{DM-1} (Ma)	T _{DM-2} (Ma)
<i>Calc-alkaline rocks</i>																			
Nasrin	S-2839	Gabbro, 49.0	630	25.9	926.4	0.081	0.703752	12	0.70303	6.69	30.07	0.1345	0.512614	7	−0.5	−0.32	4.5	1031	
Nasrin	S-2847	Gabbro, 53.2	630	37.0	688.4	0.155	0.704319	9	0.70292	4.33	19.18	0.1365	0.512630	7	−0.2	−0.31	4.7	1026	
Zreir	S-4563	Granodior. 65.7	630	51.9	670.8	0.224	0.706340	9	0.70433	3.47	20.58	0.1019	0.512388	6	−4.9	−0.48	2.7	1039	1198
Rehavam	A-39	Granite, 73.7	630	51.8	295.5	0.507	0.708910	11	0.70435	2.12	9.31	0.1377	0.512520	8	−2.3	−0.30	2.4	1262	1035
Rehavam	A-44	Granite, 74.0	630	56.1	252.6	0.643	0.709279	12	0.70351	1.42	6.16	0.1394	0.512528	8	−2.1	−0.29	2.5	1274	1025
Ahdar	S-2902	Granodior. 66.7	610	78.4	451.8	0.502	0.707501	9	0.70313	3.98	22.87	0.1052	0.512479	8	−3.1	−0.47	4.0	943	1057
Ahdar	S-2911	Granite, 70.9	610	91.6	259.0	1.024	0.713769	12	0.70486	4.00	19.61	0.1233	0.512532	7	−2.1	−0.37	3.6	1042	996
Lathi	S-1617	Granite, 72.0	607	60.9	174.5	1.011	0.713471	13	0.70472	6.97	32.47	0.1298	0.512569	7	−1.3	−0.34	3.8	1055	946
<i>Alkaline rocks</i>																			
Girgar	S-1561	Syenogran. 73.2	603	74.3	54.8	3.94	0.736416	11	0.70257	9.44	41.10	0.1389	0.512681	6	0.8	−0.29	5.3	955	779
Girgar	S-1569	Syenogran. 74.0	603	104.0	90.4	3.34	0.735157	10	0.70644	11.64	56.62	0.1243	0.512589	6	−1.0	−0.37	4.6	956	907
Yehoshafat	A-37	Afs granite, 74.3	605	104.5	58.1	5.23	0.760061	11	0.71496	4.04	23.06	0.1059	0.512483	7	−3.0	−0.46	4.0	943	1051
TimnaB	MB-109	Monzodior. 52.8	610	58.4	855.0	0.20	0.70511		0.70339	5.60	33.20	0.1020	0.51242		−4.3	−0.48	3.1	996	
TimnaB	MB-206	Monzodior. 55.4	600	84.1	549.0	0.44	0.70713		0.70333	5.68	33.50	0.1025	0.51249		−2.9	−0.48	4.3	909	
TimnaB	MB-115	Afs granite, 75.6	610	139.0	23.4	17.40	0.8468		0.69543	4.53	27.10	0.1011	0.51244		−3.9	−0.49	3.6	960	1113
Sahara	S-1600	PA granite, 74.7	608	113.1	7.6	44.78	1.131623	14	0.74332	8.82	41.58	0.1282	0.512636	6	0.0	−0.35	5.3	917	837
Umm-Ifai	S-4543	Syenogran. 73.4	586	126.4	102.4	3.58	0.738951	9	0.70902	8.34	43.27	0.1165	0.512570	7	−1.3	−0.41	4.7	910	926
Umm-Ifai	S-4546	Syenogran. 71.8	586	106.0	116.3	2.64	0.729803	8	0.70772	10.01	53.12	0.1139	0.512558	9	−1.6	−0.42	4.6	905	942
Sharm	S-1384	Afs granite, 73.6	594	146.1	49.9	8.55	0.792505	10	0.72010	15.85	97.30	0.0985	0.512503	8	−2.6	−0.50	4.8	856	1009
Sharm	S-1529	Afs granite, 69.8	594	96.0	83.1	3.35	0.733379	11	0.70500	21.04	99.50	0.1278	0.512553	8	−1.7	−0.35	3.6	890	969
Katharina	D163	Syenogran. 74.0	590	220.5	91.29	7.01	0.758037	8	0.69904	6.34	32.57	0.1177	0.512519	3	−2.3	−0.40	3.6	1002	1010
Katharina	D165	Syenogran. 74.6	590	238.3	86.75	7.98	0.767362	8	0.70020	7.26	36.33	0.1208	0.512546	3	−1.8	−0.39	3.9	991	971
Katharina	IL-66	Qtz monz. 61.2	590	53.8	396.9	0.37	0.706085	7	0.70300	10.97	62.42	0.1062	0.512571	3	−1.3	−0.46	5.5	822	911
Katharina	IL-161	Qtz syenite, 64.1	590	99.6	305.3	0.94	0.710773	7	0.70284	12.08	72.82	0.1003	0.512503	3	−2.6	−0.49	4.6	870	1012
Bimodal dykes	A196-1	Trachydol. 50.8	595	70.0	457.1	0.44	0.708304	10	0.70458	6.64	31.82	0.13	0.512502	10	−2.7	−0.36	2.7	1128	
"	N-1	Trachydol. 52.8	595	40.7	698.7	0.17	0.707539	14	0.70612	5.63	27.68	0.1230	0.512486	14	−3.0	−0.37	2.6	1115	
"	147-2	Rhyolite, 73.3	595	86.3	54.9	4.58	0.773803	17	0.73529	8.14	40.59	0.1212	0.512476	15	−3.2	−0.38	2.5	1111	1083

(1) Samples IL-66 and IL-161 are from the Katharina Ring Dike.

(2) Data from the Timna complex (Timna^B) after Beyth et al., 1994. In this work 2σ values are not reported.

(3) The Nd model ages were calculated according two-stage model for felsic rocks (TDM-II) and single-stage model for mafic rocks (TDM-I).

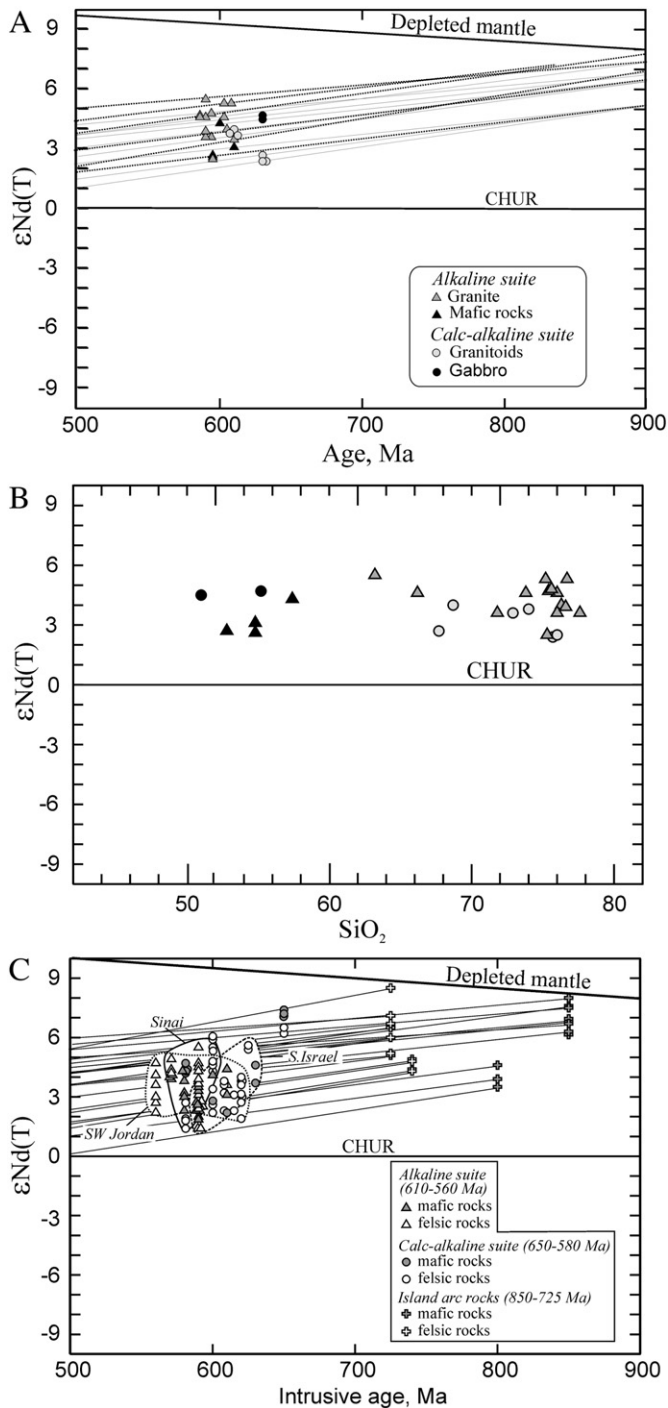


Fig. 8. A, $\epsilon_{Nd}(T)$ vs. intrusive age (Ma) diagram for representative igneous rocks from the CA and Alk suites (see Table 3); evolutionary lines for the ϵ_{Nd} values are shown for most samples (dashed and solid lines for Alk and CA rocks respectively). B, $\epsilon_{Nd}(T)$ vs. SiO_2 diagram for the same samples. C, $\epsilon_{Nd}(T)$ vs. intrusive age (Ma) diagram for post-collisional CA and Alk igneous suites and for island arc metaigneous rocks from the Sinai Peninsula, Eastern Desert (Egypt), S Israel, and SW Jordan (data from Tables 3 and 2-SD, Supplementary data).

are characteristic of both mafic and silicic rocks of the CA suite. The first is the occurrence of numerous samples with $Eu/Eu^* > 1$ (Fig. 1-SD, online Supplementary data) indicating the presence of cumulus crystals of plagioclase and possibly some mafic minerals (Fig. 2-SD) and, consequently, the significant role of crystal fractionation in the formation of intermediate and silicic rocks. The other feature is the abundance of mafic microgranular enclaves, mafic schlierens and rare synplutonic mafic dykes that are especially common in

granitoids with lower silica content (granodiorite, quartz monzonite) and granite from some of the complex plutons. Such traits are commonly interpreted as evidence of mafic and silicic magma mixing that resulted in formation of hybrid melts (e.g., Sparks and Marshall, 1986; Fernandes and Barbarin, 1991; Litvinovsky et al., 1995; Perugini and Poli, 2000; Bonin, 2004). Thus two alternative processes, fractional crystallization and magma mixing, operated during the formation of the CA granitoids. The problem is to assess the role of each process.

Duchesne et al. (1998) demonstrated on the basis of carefully studied Tismana pluton, that both processes were involved in formation of a complex shoshonitic suite ranging in composition from monzodiorite to granite. Fractional crystallization was accompanied by magma mixing; in so doing, mixing occurred between parent mafic liquid and granite melt, as well as between liquids at various stages of evolution, which is called endo-hybridization. It is likely that endo-hybridization occurred also in the Sinai region; however, lack of detailed data makes us restrict ourselves to the qualitative estimation of the role of fractional crystallization and mixing at different stages of the CA suite evolution.

The overlap in REE patterns of gabbro and granitic rocks (Fig. 10A) argues against fractional crystallization as the dominant process in magma evolution. We performed mass-balance calculations to estimate the role of fractional crystallization and magma mixing processes in the formation of the CA suite. The least-square modeling of fractional crystallization of an average CA gabbroic magma showed that none of the combinations of fractionated mineral assemblages

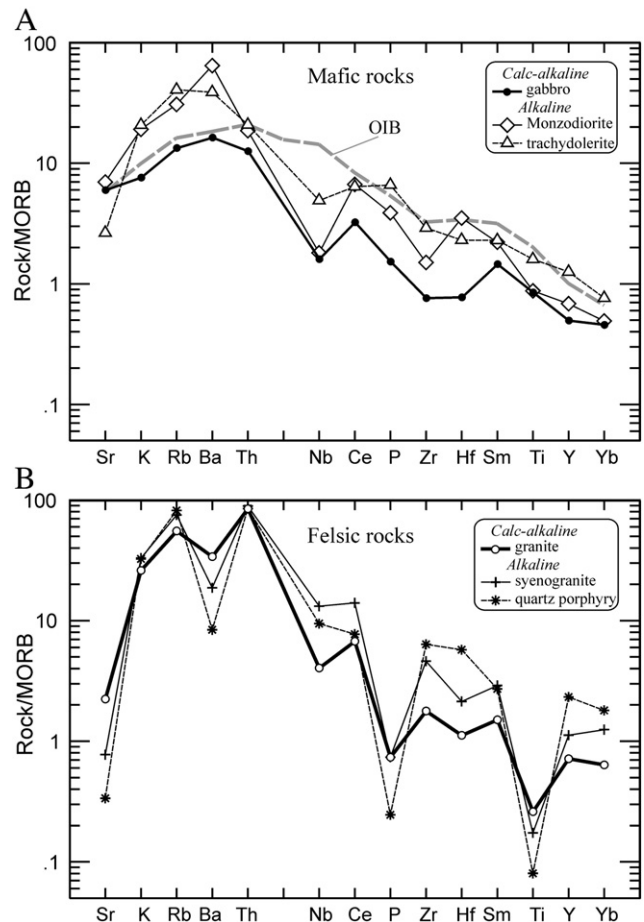


Fig. 9. MORB-normalized multi-element diagrams for mafic (A) and felsic (B) plutonic and dyke rocks from the Sinai Peninsula and southern Israel. OIB = oceanic island basalt composition (Sun and McDonough, 1989).

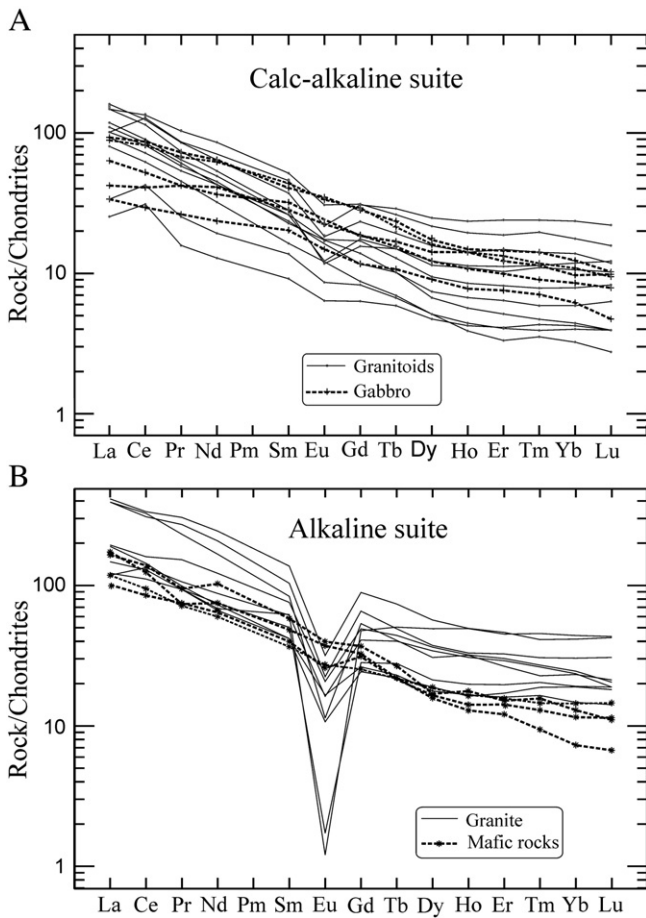


Fig. 10. REE patterns: A, for CA granitoids and related gabbro; B, for Alk granites and coeval mafic rocks.

can generate the average granodiorite composition. The lowest sum of squares of residuals is > 23.

Mass-balance calculation of mixing of gabbro and the average granite from the complex granodiorite–granite plutons (Table 5) demonstrates that the mixing model is realistic. Sum of squares of residuals is 0.75. The major element modeling was augmented by model calculation for selected trace elements; all of them, except of Ba, yielded consistent results (Table 4). The mass-balance calculation shows that granodiorite could have crystallized from a hybrid melt produced by mixing of ~15% gabbroic and 85% granite magmas. Thus the CA suite cannot be regarded as an evolved suite formed by fractional crystallization of the gabbroic magma. Although it follows from the foregoing section that granite melts are related to mafic magmas/rocks, production of intermediate melts in this suite occurred mostly by magma mixing.

Some of the granite magmas may have originated at later stages as a result of fractional crystallization of hybrid granodiorite melt. In particular, least-square modeling (Table 6) shows that highly differentiated CA granite making up the Mandar and Lathi plutons (Fig. 1, Table 2) could be readily produced by fractional crystallization of 21% plagioclase (25% An), ~7% amphibole and 2% magnetite from the granodiorite. The residual granite melt constitutes about 70% of the parental magma volume.

6.2.2. Alkaline suite

6.2.2.1. Provenance of A-type granite magmas. Genetic relations between mafic and felsic rocks in the Alk igneous suite from the northernmost ANS were discussed by many authors (Stern and

Table 5
Mass-balance calculations for the model of mixing.

Components	End-members		Daughter rocks		
	Basic magma	Silicic magma	Granodiorite		
	Gabbro	Granite complex plutons	Observed	Calculated	Diff*Wt
<i>n</i>	6	9	16		
wt.%					
SiO ₂	48.49	71.07	66.96	67.92	-0.38
TiO ₂	1.24	0.39	0.56	0.51	0.05
Al ₂ O ₃	17.26	14.89	15.98	15.22	0.38
FeO	14.01	2.84	4.14	4.39	-0.26
MnO	0.14	0.06	0.08	0.07	0.01
MgO	5.77	0.84	1.37	1.53	-0.15
CaO	8.83	1.98	2.93	2.93	0.00
Na ₂ O	2.97	3.94	4.39	3.80	0.59
K ₂ O	1.11	3.92	3.41	3.53	-0.12
P ₂ O ₅	0.18	0.07	0.18	0.09	0.09
Sum of squares of residuals					0.75
End-members fraction, %:					
Basic				13.9	
Acid				86.1	
ppm					Residual
Rb	26	111	88	99	-11
Sr	698	269	406	329	77
Ba	317	680	812	620	183
Nb	6	14	13	13	0.0
Y	14	22	20	21	-1.0
Ga	20	16	18	17	1.0
La	14	33	32	30	2.0
Ce	32	68	69	62	7.0
Nd	19	26	30	25	5.0
Sm	5	5	6	5	1.0
Eu	1.4	1	1.4	1.0	0.4
Gd	4	4	5	4	1.0
Dy	3	4	4	4	0.0
Er	1.8	2.1	2.2	2.1	0.1
Yb	1.5	2.2	2.1	2.1	0.0

(1) Major elements are recalculated to total = 100% volatile free.

(2) The calculations were conducted by the IGPET-06 program with the average compositions of rocks: gabbro (Shahira, Nasrin, Imlaha plutons); granite from the granodiorite–granite plutons (Rahba, Ahdar, Sama, Hibran-Miar plutons); granodiorite (Rahba, Ahdar, Sama, Abu Khsheib, Sulaf and Tawla plutons).

(3) Nb and Ga are calculated based upon proportion of basic and silicic end-members obtained by the mass-balance calculation.

Voegeli, 1987, 1995; Beyth et al., 1994; Kessel et al., 1998; Mushkin et al., 2003; Jarrar et al. 2003, 2008). In all listed papers preference is given to high extent fractional crystallization of mafic magma as the dominant process for the generation of alkaline granite magma. The model is supported by indistinguishable U–Pb ages of mafic and felsic rocks (Beyth et al., 1994; Be'eri-Shlevin et al., 2009a) and by convincing evidence from composite dykes attesting coexistence of mafic and silicic magmas (Stern and Voegeli, 1987; Katzir et al., 2007b). The above discussed geochemical data (Section 6.1.2; Fig. 9) and disposition of REE patterns of mafic rocks and granites in the Alk suite (Fig. 10B) also advocate genetic links between felsic and mafic rocks. Unfortunately, this body of evidence remains ambiguous since both radiogenic and stable isotope ratios cannot distinguish the contribution of mantle vs. young juvenile crust sources to the alkaline granite magmas from the ANS. Nevertheless generation of A-type silicic magma from a K-rich basalt source is preferable.

Of the two possible processes, fractional crystallization and partial melting, the former is less probable since this process cannot account for the absence of rocks of intermediate composition in the alkaline, characteristically bimodal igneous suite. Study of rare trachydacite and trachyandesite in composite dykes showed that these are hybrid rocks formed by mixing of trachydolerite and rhyolite magmas (Katzir

Table 6

Results of least-square modeling of fractional crystallization of the granodiorite magma, with the trace element testing.

wt.%	Parent		Daughter		Residual
	Granodiorite		CA granite		
			Observed	Calculated	
SiO ₂	67.08	73.69	73.21	0.48	
TiO ₂	0.57	0.35	0.51	-0.16	
Al ₂ O ₃	16.01	14.13	14.12	0.01	
FeO ¹	4.14	1.71	1.70	0.01	
MnO	0.08	0.05	0.11	-0.06	
MgO	1.37	0.54	0.79	-0.25	
CaO	2.93	1.21	0.93	0.28	
Na ₂ O	4.4	3.74	3.99	-0.25	
K ₂ O	3.42	4.58	4.64	-0.06	
Fractionating minerals, wt.%	Plagioclase				21
	Hornblende				6.9
	Magnetite				1.7
Residual melt, wt.%					70.4
Sum residuals squared					0.242
Trace element testing					
ppm	Parent		Daughter		Residual
	Granodiorite		CA granite		
			Observed	Calculated	
Rb	88	102	123	-21	
Sr	406	221	305	-84	
Ba	812	695	1033	-338	
Nb	13	13	17	-4	
Y	20	20	22	-2	
Ga	18	15	14	1	
La	32	37	39	-2	
Ce	69	75	84	-9	
Nd	30	31	32	-1	
Sm	6	6	6	0.0	
Eu	1.4	1.1	1.0	0.1	
Gd	5	5	4	1	
Dy	4	4	3	1	
Er	2.2	2.3	1.9	0.4	
Yb	2.1	2.3	2.0	0.3	

(1) Major elements are calculated to 100% volatile free.

(2) Averages: granodiorite ($n = 16$); granite from the Mandar and Lathi plutons ($n = 10$).

(3) Sources of partition coefficient values: Arth, 1976; Nash and Crecraft, 1985; Rollinson, 1993.

et al., 2007b). The geochemical modeling of the fractional crystallization process requires assumptions that turn the results highly speculative (i.e. Kessel et al., 1998; Mushkin et al., 2003; Jarrar et al., 2008). On the other hand, it is likely that partial melting of rocks that are similar in chemical composition to trachydolerite and monzodiorite from the Alk suite (Table 2) can result in generation of typical A-type granite magmas. This was demonstrated by melting experiments performed by Sisson et al. (2005). One of the three basalt samples (AD19-93) used in their experiments is fairly similar to the Alk mafic rocks under discussion, in particular in SiO₂ (50.74%), TiO₂ (1.25%), MgO (4.52%), Na₂O (3.76%) and K₂O (2.32%) contents. Partial melting of this sample at 700 MPa to an extent of ~20% produced granite melts with 3.2 to 3.5 wt.% Na₂O and 4.7 to 5.94 wt.% K₂O. The experimental data show that partial melting of K-rich basalt rocks in the middle and lower crust may produce significant amount of A-type granite magma that can be easily separated and emplaced at shallow levels. The partial melting process explains the absence of igneous rocks of intermediate composition, as well as the very rare occurrence of co-genetic mafic rocks in plutonic suites. It also accounts for the highly pronounced negative Eu anomalies in alkaline granite (Eu/Eu* < 0.5, see Figs. 4B, 10B and 1-SD, online Supplementary data). According to Sisson et al. (2005, Table S1), in all runs proportion of plagioclase in the residual phase was ≥ 50%. This likely caused the deficit of Eu in the partial melts.

6.2.2.2. Genetic relations between syenogranite, Afs and PA granite. Field observations show that the formation of the granite suite commenced with emplacement of syenogranite melts. The chemical composition of syenogranite is fairly homogenous in each single pluton, but distinct in different plutons (Fig. 7). In plutons consisting of syenogranite the rock composition shows systematic decrease in ΣREE accompanied by increase in negative Eu anomaly in the following order: Dahab, Umm-Ifai, Katharina, Iqna. Decrease in Eu/Eu* values is accompanied by decrease in CaO, Sr, Ba, Al₂O₃, Nb and, less clear, Zr (Fig. 11). The Dahab pluton is not shown in the plots since it falls out of the common trend, probably due to the effect of mafic enclaves irregularly scattered in the pluton (Table 1). The systematic geochemical trends in syenogranites from different plutons (Fig. 11) imply fractionation of feldspar, minor accessories and Fe-Ti oxides from the least differentiated magma, represented by Umm-Ifai syenogranite. These trends suggest that batches of the syenogranite magma were separated from magma reservoir(s) at different stages of differentiation and emplaced at higher levels forming individual plutons.

Comparison of syenogranite and Afs (+ PA) granites in the plutons that incorporate two or more rock types (Fig. 12) demonstrates that in each individual pluton the Afs granite could form by fractional crystallization of two feldspars and minor mafic minerals from the syenogranite magma. This suggests that batches of syenogranite magma that formed separate plutons were subjected to further fractional crystallization during or after emplacement. The evolution of syenogranite magma resulting in production of Afs granite was portrayed in detail in the vertically zoned Katharina pluton (Katzir et al., 2007a).

6.3. Tectonic setting during the calc-alkaline and alkaline suite formation

The specific features and complex character of post-collisional magmatism became a topical issue during the last decade (e.g., Liégeois, 1998; Bonin, 2004; Whalen et al., 2006). According to Liégeois (1998), the post-collisional period begins after completion of collision of two or more 'continental' plates and concomitant HT metamorphism. Post-collisional magmatism occurs in an intracontinental environment, but still with large horizontal terrane movements along mega-shear zones. One of the main characteristics of post-collisional magmatism is the abundance of high-K calc-alkaline granitoids. It often ends with silica-oversaturated alkaline-peralkaline magmatism, heralding the quieter intraplate period.

Most authors argue that the high-K calc-alkaline and alkaline series should represent different tectonic settings, and if they occur in the same region, they are generally successive but not contemporaneous (Liégeois et al., 1998; Bonin, 2004, 2007). However, a number of works point to an essential overlap in time of post-collisional CA and Alk igneous suites in various regions of the world. In addition to the well-known Pan-African stratoid granites of Madagascar (Nédélec et al., 1995), some other examples should be mentioned. Significant overlap in time was established: (1) in Transbaikalia, Russia, for the high-K calc-alkaline Angara-Vitim batholith (ca. 150,000 km²; 330–285 Ma) and for the closely associated plutonic suites of alkaline quartz syenite-granite (305–285 Ma) (U-Pb data by Yarmolyuk et al., 1997; Kovalenko et al., 2004; Tsygankov et al., 2007); (2) in northern Mongolia, for the Early Mesozoic Khentei-Daurian calc-alkaline batholith and the closely spaced rift-related alkaline-peralkaline granite plutons; they were emplaced during the same time span of 227 Ma to 207 Ma (U-Pb ages; Yarmolyuk et al., 2002); (3) in NW China (Ulungu River), for closely associated calc-alkaline (I-type granite) and peralkaline granite plutons (Rb-Sr ages, 300–280 Ma; Han et al., 1997; Chen and Jahn, 2004); (4) in the Yangtze block of South China, Neoproterozoic I-type (high-K calc-alkaline) and A-type granites have similar SHRIMP zircon U-Pb ages of ~800 Ma (Zhao et al., 2008), and (5) in western Newfoundland, Whalen et al. (2006)

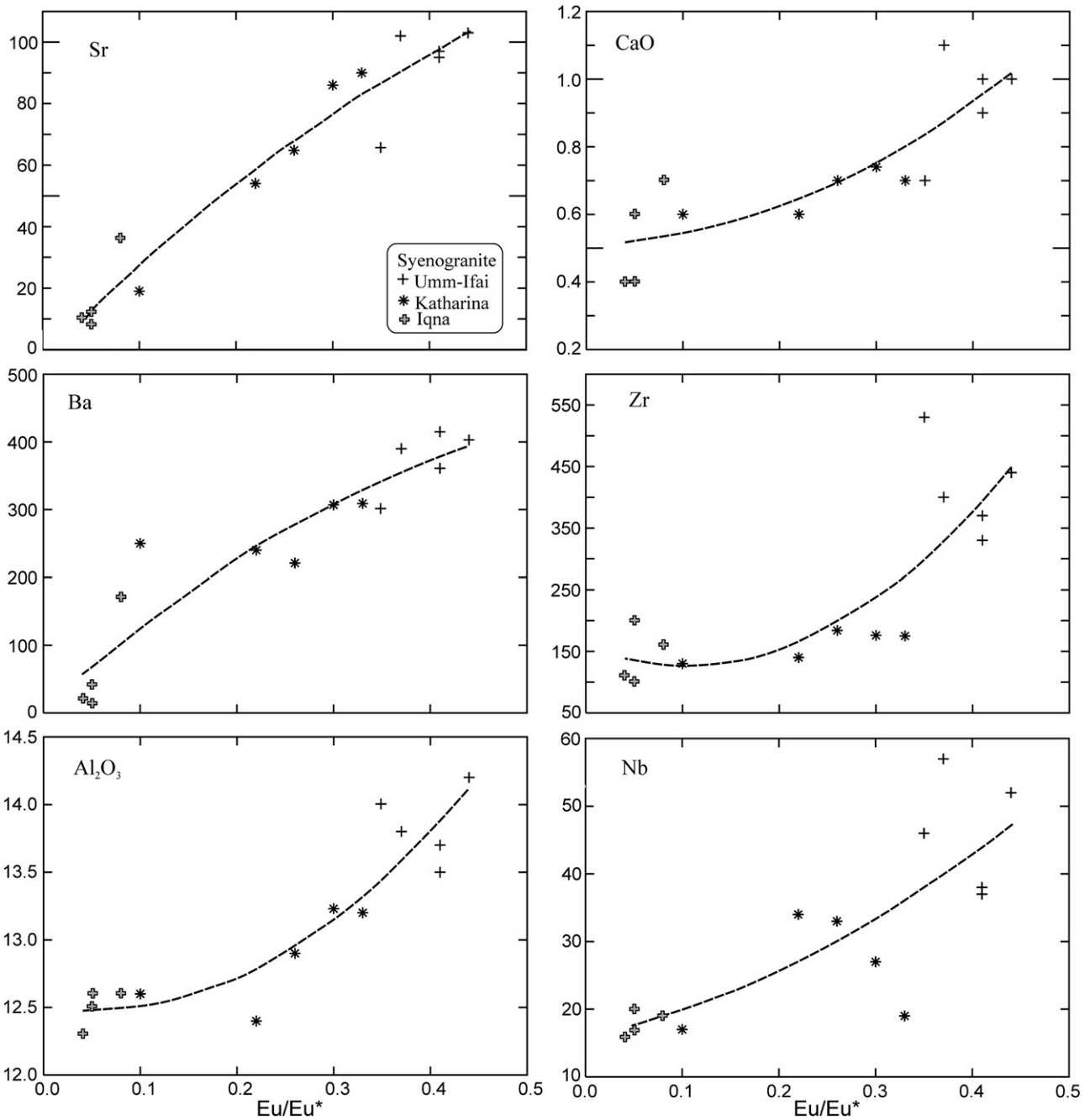


Fig. 11. Eu/Eu^* vs. Sr, Ba, Al_2O_3 , CaO, Zr, and Nb diagrams for typical syenogranite plutons. The diagrams present evidence of the dominant role of fractional crystallization in the evolution of the syenogranite magma.

described concurrent, but extremely diverse Silurian post-collisional magmatism that occurred immediately after formation of arc-like plutonic suites. During a period of ~8 m.y., from 435 to 427 ± 3 Ma, large volumes of magmas with diverse compositions were intruded in time periods almost completely or partially overlapping. These magmas include calc-alkaline medium-K and low-K gabbro and diorite with tonalite and granodiorite, calc-alkaline medium- and high-K granite, monzogranite, both metaluminous and peraluminous and typical A-type granites, including peralkaline granite with arfvedsonite and riebeckite.

Thus, the prolonged and contemporaneous emplacement of CA and Alk suites in the Sinai Peninsula is not unique. The distinctive feature of this region is that it constitutes the northernmost part of the ANS that formed as a result of accretion of juvenile arc terranes on a

territory of about 1600 by 1000 km (Kröner et al., 1987; Pallister et al., 1988; Ayalew et al., 1990; Kröner et al., 1990; Stern and Kröner, 1993; Genna et al., 2002; Stern, 2002). The post-collisional magmatic stage throughout the ANS commenced with the emplacement of high-K calc-alkaline batholiths (Bentor, 1985; Stoesser and Camp, 1985; Stern and Abdelsalam, 1998; Moghazi et al., 1998; Moghazi, 2002; Jarrar et al., 2003). The emplacement of CA suites lasted over a period of about 40–45 m.y., but during the second half of this period, from 608 Ma to 590 Ma, both CA and Alk igneous suites formed in parallel at least at the Sinai Peninsula (Beyth et al., 1994; Moghazi et al., 1998; Be'eri-Shlevin et al., 2009a).

Looking for appropriate tectonic settings that could cause superposition of magmatic events, one should take into account that the Late Neoproterozoic post-collisional high-K calc-alkaline

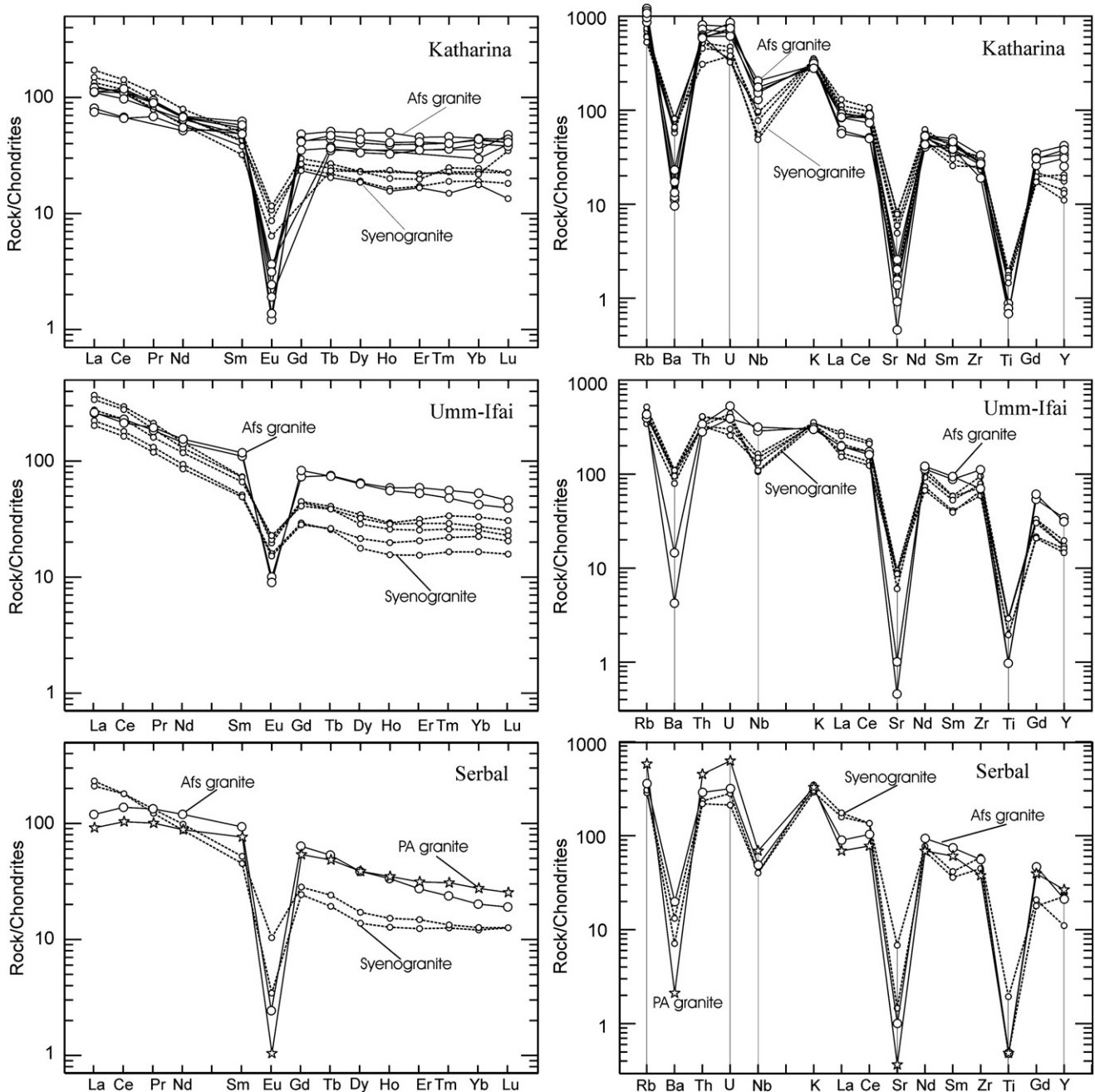


Fig. 12. REE patterns and chondrite-normalized multi-element diagrams for syenogranite and Afs (+PA) granites from selected plutons. Chondrite values from Sun and McDonough (1989).

batholiths are abundant not only in the ANS, but also in many regions throughout North Africa, in which the Pan-African (Neoproterozoic) orogenesis was manifested. The largest and most abundant batholiths occur at the Tuareg shield that is situated to the west of the ANS and formed in the Neoproterozoic by extensive interaction of continental plates, mainly the West African and East Saharan cratons (Black and Liégeois, 1993; Abdelsalam et al., 2002). Like the ANS, most of the post-collisional batholiths in the Tuareg shield were emplaced over the period of 635–580 Ma (Liégeois et al., 1998 and references therein). Unlike the ANS, alkaline–peralkaline granites and rhyolites of the Tuareg shield (e.g., Adrar des Iforas, Mali) intruded noticeably later, at 560–540 Ma.

Judging from the chemical data and mineralogical characteristics given in the cited papers, the main granitic rock types, both calc-

alkaline and alkaline, are very similar in the Tuareg and the northern Arabian–Nubian Shields. However, the negative $\varepsilon_{\text{Nd}(T)}$ values in granitoids of the Tuareg shield suggest significant involvement of ancient continental crust material in the magma generation (see Table 1 in Liégeois et al., 1998).

The ANS, along with the adjacent terranes of the northern East African Orogen, experienced collision (Fig. 13A) that was completed, as a whole, by ~640 Ma (Stern, 1994). As a result of collision, both the juvenile arc crust and the subarc lithospheric mantle were thickened; Avigad and Gvirtzman (2009) estimated that at 630 Ma crustal and lithospheric thicknesses exceeded 50 and 150 km, respectively. This induced gravitational and thermal instability (Marotta et al., 1998). The onset of extensive melting was probably caused by thermal restoration of the heat flow depressed by the preceding subduction

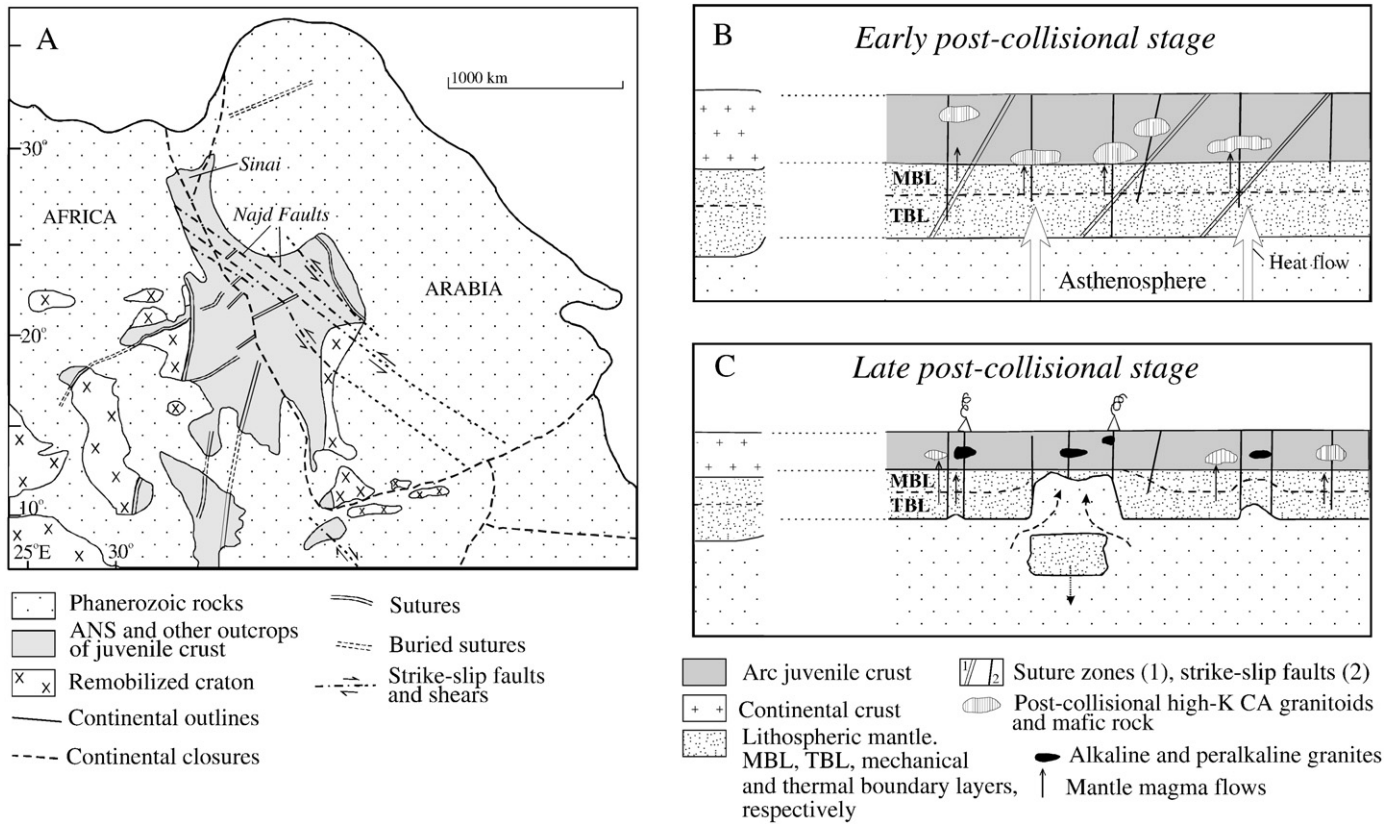


Fig. 13. A, Simplified tectonic map of the northern East African Orogen with continental fragments shown as configured at the end of Precambrian (after Stern, 1994). B and C, Idealized sections of the juvenile arc terrane at early and late post-collisional stages respectively (see discussion in the text). The crust and lithospheric mantle thickness is shown off scale. The lithosphere "layers", Mechanical Boundary Layer (MBL) and Thermal Boundary Layer (TBL), after Black and Liégeois, 1993. Vertical lines are shear zones.

and plate collision (Liégeois et al., 1998). Temperature rise in the lower Thermal Boundary Layer of the lithospheric mantle, previously enriched in incompatible elements, resulted in voluminous basalt magma generation. Underplating and intrapating of the crust by the ascending basalt magmas caused large-scale melting of the juvenile crust, magma mingling–mixing, differentiation and formation of calc-alkaline plutonic suite (Fig. 13B). It is likely that emplacement of basalt magmas was controlled by trans-lithospheric shear zones. Berhe (1990) noted that the entire East African Orogen was affected by NW–SE trending strike-slip faults and suggested that these resulted from an oblique collision.

The next post-collisional stage commenced ~20 m.y. later, when thickness of both lithospheric mantle and crust decreased. At this stage, CA and Alk igneous suites formed concurrently, although from distinct sources. We suggest that the Thermal Boundary Layer (TBL) of the lithospheric mantle continued to interact with the underlying asthenosphere, so the upper margin of TBL moved upward (Fig. 13C). Further asthenospheric upwelling resulted in thermal corrosion of the lithospheric mantle and, lastly, to its delamination between neighbouring shear zones (Liégeois et al., 1998) as shown in Fig. 13C. Probably delamination caused sharp increase of extensional tectonism and Alk magmatic activity (late Alk sub-stage, 595–580 Ma). The latter was exhibited in volcanic outpouring, formation of alkali rich silica-oversaturated ring complexes and large bimodal dike swarms. Repeated intrapating of alkali basalt magmas could cause partial melting of recently intruded and crystallized material of similar composition; this resulted in formation of Alk granites and rhyolites.

The proposed model is utterly simplified, but it gives, to a first approximation, an understanding of the close association of CA and Alk granites in space and time despite their different mantle sources. Also it provides explanation for the combination of overlap in time

between CA and Alk suite in the regional scale vs. the successive emplacement of CA, then Alk granitoids in the local scale (see above, Section 2). Obviously the real situation should include mixing of lithospheric and asthenospheric sources and generation of silicic magmas that produce chemically similar granites in the course of formation of CA and Alk suites (compare highly differentiated CA granite from the Lathi and Mandar plutons with Alk syenogranite from the Girgar and Umm-Ifai plutons in Table 2 and Fig. 3-SD, online Supplementary data). Mixing of two mantle sources (along with subsequent magma differentiation) may be the reason for the similarity of alkaline and "highly fractionated" calc-alkaline granites (Sylvester, 1989; Bonin, 2004 and references therein).

7. Conclusions

- Two geochemical types of Neoproterozoic post-collisional igneous rocks, calc-alkaline (CA) and alkaline–peralkaline (Alk), are abundant and closely spaced in the Sinai Peninsula (Egypt) and southern Israel. Extensive ion-probe U–Pb dating of zircons (Be'eri-Shlevin et al., 2009a) enabled to establish a significant, about 20 m.y. long, overlap in the ages of CA and Alk rocks. Along with partial overlap in the regional scale, emplacement of CA granitoids preceded formation of Alk plutons locally in the scale of individual areas of hundreds of square kilometers.
- Despite close association in space and time, CA and Alk granitoids are clearly distinguished in some major and trace element characteristics. This was demonstrated for 27 key plutons and plutonic complexes.
- Felsic and mafic igneous rocks from the CA and Alk suites are characterized by similar positive $\epsilon_{\text{Nd}(T)}$ values varying from +1.5 to +6 Nd and oxygen isotope ratios. Isotope ratios cannot unequivocally trace the provenance of silicic magmas since juvenile

- crust is abundant throughout the region. Elemental geochemical data suggest significant proportion of mantle component in CA granitoids.
- Granodiorite magmas in the CA suite were likely formed by mixing of granite and gabbro end-members in proportion of about 85 and 15%, respectively. Fractional crystallization of the hybrid granodiorite could play an important role in the origin of younger highly differentiated CA granite magmas.
 - Alkaline granite magma could be produced by partial (~20%) melting of related mafic rocks that are compositionally similar to K-rich basalt. In the Alk suite, the more differentiated felsic rock types evolved mostly by fractional crystallization of the initial least differentiated syenogranite melt.
 - A post-collisional tectonic setting that promoted contemporaneous calc-alkaline and alkaline–peralkaline granitoid magmatism should involve extensive heat and material transfer from the asthenosphere into the lithospheric mantle and lower crust. In the northern ANS such asthenospheric flow began at ~615 Ma and resulted in concurrent tapping of two mantle sources: the upper mechanical boundary layer of the lithospheric mantle and the thermal boundary layer at the base of the lithosphere enriched in asthenospheric components.

Acknowledgements

The study was supported by the Israel Science Foundation grant # 142/02, the Ministry of National Infrastructure and Energy, Israel grant ES-18-2008, the Ministry of Science and Technology, Israel grant 3-3571, and by the National Science Council (NSC), Taiwan, grants NSC96-2923-M-001-001-MY3, NSC96-2116-M-001-004; NSC97-2752-M-002-003-PAE, and NSC97-2116-M-001-011. We are grateful to R. Rudnick, J. P. Liégeois and anonymous reviewer for valuable recommendations that provided considerable improvement of the manuscript. Also authors are indebted to Yaron Be'eri-Shlevin for fruitful cooperation in the interpretation of the U–Pb and oxygen isotope data.

Appendix A. Supplementary data

Supplementary data associated with this article can be found, in the online version, at doi:10.1016/j.chemgeo.2009.09.010.

References

- Abdelsalam, M.G., Liégeois, J.P., Stern, R.J., 2002. The Saharan metacraton. *Journal of African Earth Sciences* 34, 119–136.
- Ali, B.H., Wilde, S.A., Gabr, M.M.A., 2009. Granitoid evolution in Sinai, Egypt, based on precise SHRIMP U–Pb zircon geochronology. *Gondwana Research* 15, 38–48.
- Arth, J.G., 1976. Behavior of trace elements during magmatic processes – a summary of theoretical models and their applications. *Journal of Researches of U.S. Geological Survey* 4, 41–47.
- Avigad, D., Gvirtzman, Z., 2009. Late Neoproterozoic rise and fall of the northern Arabian–Nubian Shield: the role of lithospheric mantle delamination and subsequent thermal subsidence. *Tectonophysics*. doi:10.1016/j.tecto.2009.04.018.
- Ayalew, T., Bell, K., Moore, J.M., Parrish, R.R., 1990. U–Pb and Rb–Sr geochronology of the Western Ethiopian Shield. *Geological Society of America Bulletin* 102, 1309–1316.
- Be'eri-Shlevin, Y., Katzir, Y., Whitehouse, M., 2009a. Post-collisional tectono-magmatic evolution in the northern Arabian–Nubian Shield (ANS): time constraints from ion-probe U–Pb dating of zircon. *Journal of Geological Society, London* 166, 71–85.
- Be'eri-Shlevin, Y., Katzir, Y., Valley, J.W., 2009b. Crustal evolution and recycling in a juvenile continent: oxygen isotope ratio of zircon in the northern Arabian Nubian Shield. *Lithos* 107, 169–184.
- Bentor, Y.K., 1985. The crust evolution of the Arabo-Nubian Massif with special reference to the Sinai Peninsula. *Precambrian Research* 28, 1–74.
- Bentor, Y.K., Eyal, M., 1987. The Geology of Southern Sinai, Its Implication for the Evolution of the Arabo-Nubian Massif. Israeli Academy of Sciences and Humanities, Jerusalem. 484 pp.
- Berhe, S., 1990. Ophiolites in Northeast and East Africa: implications for Proterozoic crustal growth. *Journal of the Geological Society, London* 147, 41–57.
- Beyth, M., Stern, R.J., Altherr, R., Kröner, A., 1994. The Late Precambrian Timna igneous complex Southern Israel: evidence for comagmatic-type sanukitoid monzodiorite and alkali granite magma. *Lithos* 31, 103–124.
- Bielski, M., 1982. Stages in the Evolution of the Arabian–Nubian Massif in Sinai. Ph.D. thesis, Hebrew University of Jerusalem. 155 pp.
- Black, R., Liégeois, J.P., 1993. Cratons, mobile belts, alkaline rocks and continental lithospheric mantle: the Pan-African testimony. *Journal of Geological Society, London* 150, 89–98.
- Bonin, B., 2004. Do coeval mafic and felsic magmas in post-collisional to within-plate regimes necessarily imply two contrasting, mantle and crustal, sources? A review. *Lithos* 78, 1–24.
- Bonin, B., 2007. A-type granites and related rocks: evolution of a concept, problems and prospects. *Lithos* 97, 1–29.
- Chen, B., Jahn, B.M., 2004. Genesis of post-collisional granitoids and basement nature of the Junggar Terrane, NW China: Nd–Sr isotope and trace element evidence. *Journal of Asian Earth Sciences* 23, 691–704.
- Cosca, M.A., Shimron, A., Caby, R., 1999. Late Precambrian metamorphism and cooling in the Arabian–Nubian Shield: petrology and ⁴⁰Ar/³⁹Ar geochronology of metamorphic rocks of the Elat area (southern Israel). *Precambrian Research* 98, 107–121.
- Duchesne, J.-C., Berza, T., Liégeois, J.-P., Auwera, J.V., 1998. Shoshonitic liquid line of descent from diorite to granite: the Late Precambrian post-collisional Tismana pluton South Carpathians, Romania. *Lithos* 45, 281–303.
- Eiler, J.M., 2001. Oxygen isotope variations of basaltic lavas and upper mantle rocks. In: Valley, J.W., Cole, D.R. (Eds.), *Stable Isotope Geochemistry: MSA Reviews in Mineralogy Series*, vol. 43, pp. 319–364.
- El-Nisr, S.A., El-Sayed, M.M., Saleh, G.M., 2001. Geochemistry and petrogenesis of Pan-African late- to post-orogenic younger granitoids at Shalatin–Halaib, south Eastern Desert, Egypt. *Journal of African Earth Sciences* 33, 261–282.
- El-Sayed, M.M., El-Nisr, S.A., 1999. Petrogenesis and evolution of the Dineibit El-Qulieb hyperaluminous leucogranite, Southern Desert, Egypt: petrological and geochemical constraints. *Journal of African Earth Sciences* 28, 703–720.
- El-Shafei, M.K., Kusky, T.M., 2003. Structural and tectonic evolution of the Neoproterozoic Feiran–Solaf metamorphic belt, Sinai Peninsula: implication for the closure of the Mozambique Ocean. *Precambrian Research* 123, 269–293.
- Eyal, Y., 1980. The geological history of the Precambrian metamorphic rocks between Wadi Twaiba and Wadi Um Mara, NE Sinai. *Israel Journal of Earth Sciences* 29, 53–66.
- Eyal, Y., Amit, O., 1980. The Magrish Migmatite (Northeastern Sinai) and their genesis by metamorphic differentiation triggered by a change in the strain orientation. *Israel Journal of Earth Sciences* 33, 189–200.
- Eyal, M., Bartov, Y., Shimron, A.E., Bentor, Y.K., 1980. Sinai – Geological Map, Geological Survey of Israel.
- Eyal, M., Hezkiyahu, T., 1980. Katharina Pluton – the outlines of a petrological framework. *Israel Journal of Earth Sciences* 29, 41–52.
- Eyal, Y., Eyal, M., Kröner, A., 1991. Geochronology of the Elat Terrane metamorphic basement and its implication for crustal evolution of the NE part of the Arabian–Nubian Shield. *Israel Journal of Earth Sciences* 40, 5–16.
- Eyal, M., Litvinovsky, B.A., Katzir, Y., Zanvilevich, A.N., 2004. The Pan-African high-K calc-alkaline peraluminous Elat granite of southern Israel: geology, geochemistry and petrogenesis. *Journal of African Earth Sciences* 40, 115–136.
- Fernandes, A., Barbarin, B., 1991. Elative rheology of coexisting mafic and felsic magmas: nature of resulting interaction processes. Shape and mineral fabrics of mafic microgranular enclaves. In: Didier, J., Barbarin, B. (Eds.), *Enclaves and Granite Petrology, Development in Petrology*, vol. 13. Elsevier, Amsterdam, pp. 263–275.
- Garfunkel, Z., 1999. History and paleogeography during the Pan-African orogen to stable platform transition: reappraisal of the evidence from Elat area and northern Arabian–Nubian Shield. *Israel Journal of Earth Sciences* 48, 135–157.
- Genna, A., Nehlig, P., Le Goff, E., Gguerrot, C., Shanti, M., 2002. Proterozoic tectonism of the Arabian Shield. *Precambrian Research* 117, 21–40.
- Han, B.F., Wang, S.G., Jahn, B.M., Hong, D.W., Kagami, H., Sun, Y.L., 1997. Depleted-mantle magma source for the Ulungu River A-type granites from north Xinjiang, China: geochemistry and Nd–Sr isotopic evidence, and implication for Phanerozoic crustal growth. *Chemical Geology* 138, 135–159.
- Hargrove, U.S., Stern, R.J., Kimura, J.-I., Manton, W.I., Johnson, P.R., 2006. How juvenile is the Arabian–Nubian Shield? Evidence from Nd isotopes and pre-Neoproterozoic inherited zircon in Bi'r Umk suture zone, Saudi Arabia. *Earth Planetary Science Letters* 252, 308–326.
- Jarrar, G.H., Stern, R.J., Saffarini, G., Al-Zubi, H., 2003. Late and post-orogenic Neoproterozoic intrusions of Jordan: implications for crustal growth in the northernmost segment of the East African Orogen. *Precambrian Research* 123, 295–319.
- Jarrar, G.H., Manton, W.I., Stern, R.J., Zachmann, F., 2008. Late Neoproterozoic A-type granites in the northernmost Arabian–Nubian Shield formed by fractionation of basaltic melts. *Chemie der Erde* 68, 295–312.
- Johnson, P.R., 2003. Post-amalgamation basins of the NE Arabian shield and implications for Neoproterozoic tectonism in the northern East African orogen. *Precambrian Research* 143, 321–337.
- Johnson, P.R., Woldehaimanot, B., 2003. Development of the Arabian–Nubian Shield: perspectives on accretion and deformation in the northern East African Orogen and the assembly of Gondwana. *Geological Society, London, Special Publications* 206, 289–325.
- Katz, O., Avigad, D., Matthews, A., Heimann, A., 1998. Precambrian metamorphic evolution of the Arabian–Nubian Shield in the Roded area, southern Israel. *Israel Journal of Earth Sciences* 47, 93–110.
- Katzir, Y., Litvinovsky, B.A., Eyal, M., Zanvilevich, A.N., Vapnik, Ye, 2006. Four successive episodes of Late Pan-African dikes in the central Elat area, southern Israel. *Israel Journal of Earth Sciences* 55, 69–93.
- Katzir, Y., Eyal, M., Litvinovsky, B.A., Jahn, B.-M., Zanvilevich, A.N., Valley, J.W., Beeri, Y., Pelly, I., Shimshilashvili, E., 2007a. Petrogenesis of A-type granites and origin of vertical zoning in the Katharina pluton, Gebel Mussa (Mt. Moses) area, Sinai, Egypt. *Lithos* 95, 208–228.
- Katzir, Y., Litvinovsky, B.A., Jahn, B.-M., Eyal, M., Zanvilevich, A.N., Valley, J.W., Vapnik, Ye, Beeri, Y., Spicuzza, M., 2007b. Interrelations between coeval mafic and A-type

- silicic magmas from composite dykes in a bimodal suite of southern Israel, northernmost Arabian–Nubian Shield: geochemical and isotope constrains. *Lithos* 97, 336–364.
- Kessel, R., Stein, M., Navon, O., 1998. Petrogenesis of late Neoproterozoic dikes in the northern Arabian–Nubian Shield Implication for the origin of A-type granites. *Precambrian Research* 92, 195–213.
- Keto, L.S., Jacobsen, S.B., 1987. Nd and Sm isotope variations of Early Paleozoic oceans. *Earth and Planetary Science Letter* 84, 27–41.
- Kolodner, K., 2007. The provenance of the siliciclastic section in Israel and Jordan: U–Pb dating of detrital zircons. Ph.D. thesis, Hebrew University of Jerusalem, Israel. 133 pp.
- Kolodner, K., Avigad, D., McWilliams, M., Wooden, J.L., Weissbrod, T., Feinstein, S., 2006. Provenance of north Gondwana Cambrian–Ordovician sandstone: U–Pb SHRIMP dating of detrital zircons from Israel and Jordan. *Geological Magazine* 143, 367–391.
- Kovalenko, V.I., Yarmolyuk, V.V., Kovach, V.P., Kotov, A.B., Kozlovsky, A.M., Salmnikova, E.B., Larin, A.M., 2004. Isotope provinces, mechanisms of generation and sources of the continental crust in the Central Asian Mobile Belt: geological and isotopic evidence. *Journal of Asian Earth Sciences* 23, 605–627.
- Kröner, A., Stern, R.J., Dawoud, A.S., Compston, W., Reschmann, F., 1987. The Pan-African continental margin in northeastern Africa: evidence from a geochronological study of granulites at Sabaloka, Sudan. *Earth and Planetary Science Letters* 85, 91–104.
- Kröner, A., Eyal, M., Eyal, Y., 1990. Early Pan-African evolution of the basement around Elat, Israel and Sinai Peninsula revealed by single-zircon evaporation dating, and implication for crustal accretion rates. *Geology* 18, 545–548.
- Küster, D., Liégeois, J.-P., Matukov, D., Sergeev, S., Lucassen, F., 2008. Zircon geochronology and Sr, Nd, Pb isotope geochemistry of granitoids from Bayuda Desert and Sabaloka (Sudan): evidence for a Bayudian event (920–900 Ma) preceding the Pan-African orogenic cycle (860–590 Ma) at the eastern boundary of the Saharan Metacraton. *Precambrian Research* 164, 16–39.
- Le Maitre, R.W. (Ed.), 1989. *A Classification of Igneous Rocks and Glossary of Terms*. Blackwell Scientific Publ., Oxford. 193 pp.
- Liégeois, J.P., 1998. Preface – some words on the post-collisional magmatism. *Lithos* 45, 15–17.
- Liégeois, J.P., Black, R., 1987. Alkaline magmatism subsequent to collision in the Pan-African belt of the Adrar des Iforas. *Alkaline Igneous Rocks*: In: Fitton, J.G., Upton, B.G.J. (Eds.), *Geological Society of Special Publications*, vol. 30, pp. 381–401. London.
- Liégeois, J.P., Navez, J., Hertogen, J., Black, R., 1998. Contrasting origin of post-collisional high-K calc-alkaline and shoshonitic versus alkaline and peralkaline granitoids. The use of sliding normalization. *Lithos* 45, 1–28.
- Liégeois, J.P., Stern, R.J., 2009. Sr–Nd isotopes and geochemistry of granite–gneiss complexes from the Meatiq and Hafafit domes, Eastern Desert, Egypt: no evidence for pre-Neoproterozoic crust. *Journal of African Earth Sciences*. doi:10.1016/j.jafrearsci.2009.07.006.
- Litvinovsky, B.A., Zanzilevich, A.N., Kalmanovich, M.A., 1995. Recurrent mixing and mingling of coexisting syenite and basalt magmas in the Ust'-Khilok massif, Transbaikalia, and its petrologic significance. *Petrology* 3, 115–137.
- Mathews, A., Reymer, A.P.S., Avigad, D., Cochin, J., Marco, S., 1989. Pressures and temperatures of Pan-African high grade metamorphism in the Eilat association, NE Sinai. *Israel Journal of Earth Sciences* 38, 1–17.
- Marotta, A.M., Fernandez, M., Sabadini, R., 1998. Mantle unrooting in collisional settings. *Tectonophysics* 296, 31–46.
- Meert, J.G., 2003. A synopsis of events related to the assembly of eastern Gondwana. *Tectonophysics* 362, 1–40.
- Moghazi, A.M., 1999. Magma source and evolution of Late Neoproterozoic granitoids in the Gabal El-Urf area, Eastern Desert, Egypt: geochemical and Sr–Nd isotopic constraints. *Geological Magazine* 136, 285–300.
- Moghazi, A.M., 2002. Petrology and geochemistry of Pan-African granitoids, Kab Amiri area, Egypt – implications for tectonomagmatic stages of the Nubian Shield evolution. *Mineralogy and Petrology* 75, 41–67.
- Moghazi, A.M., Andersen, T., Oweiss, G.A., El-Bouseily, A.M., 1998. Geochemical and Sr–Nd–Pb isotopic data bearing on the origin of Pan-African granitoids in the Kid area, southeast Sinai, Egypt. *Journal of Geological Society, London* 155, 697–710.
- Mushkin, A., Navon, O., Halicz, L., Heimann, A., Hartmann, G., Stein, M., 2003. The petrogenesis of A-type magmas from the Amram Massif, southern Israel. *Journal of Petrology* 44, 815–832.
- Nash, W.P., Crecraft, H.R., 1985. Partition coefficients for trace elements in silicic magmas. *Geochimica et Cosmochimica Acta* 49, 2309–2322.
- Nédélec, A., Stephens, W.E., Fallick, A.E., 1995. The Pan-African stratoid granites of Madagascar: alkaline magmatism in a post-collisional extensional setting. *Journal of Petrology* 36, 1367–1391.
- Pallister, J.S., Stacey, J.S., Fisher, L.B., Premo, W.R., 1988. Precambrian ophiolites of Arabia: geologic setting, U–Pb geochronology, Pb-isotope characteristics and implication for continental accretion. *Precambrian Research* 38, 1–54.
- Perugini, D., Poli, G., 2000. Chaotic dynamics and fractals in magmatic interaction processes: a different approach to the interpretation of mafic microgranular enclaves. *Earth and Planetary Science Letters* 175, 93–103.
- Rickwood, P.C., 1989. Boundary lines within petrologic diagrams which use oxides of major and minor elements. *Lithos* 22, 247–263.
- Rollinson, H., 1993. *Using Geochemical Data: Evaluation, Presentation, Interpretation*. Longman, New York. 352 p.
- Shimron, A.E., 1972. The Precambrian Structural and Metamorphic History of the Elat Area. Ph.D. thesis, The Hebrew University of Jerusalem. 244 pp.
- Shimron, A.E., 1984. Evolution of the Kid group, southeast Sinai Peninsula: thrusts, mélanges, and implication for accretionary tectonics during the Proterozoic of the Arabian–Nubian Shield. *Geology* 12, 242–247.
- Shpitzer, M., Beyth, M., Mathews, A., 1992. Igneous differentiation in the Late Precambrian plutonic rocks of Mt. Timna. *Israel Journal of Earth Sciences* 40, 17–27.
- Sisson, T.W., Ratajevski, K., Hankins, W.B., Glazner, A.F., 2005. Voluminous granitic magmas from common basaltic source. *Contributions to Mineralogy and Petrology* 148, 635–661.
- Sparks, R.S.J., Marshall, L., 1986. Thermal and mechanical constraints on mixing between mafic and silicic magmas. *Journal of Volcanology and Geothermal Researches* 29, 99–124.
- Stein, M., Goldstein, S.L., 1996. From plume head to continental lithosphere in the Arabian–Nubian Shield. *Nature* 382, 773–778.
- Stein, M., Navon, O., Kessel, R., 1997. Chromatographic metasomatism of the Arabian–Nubian lithosphere. *Earth and Planetary Science Letters* 152, 75–91.
- Stern, R.J., 1994. Arc assembly and continental collision in the Neoproterozoic East African orogen. Implications for the consolidation of Gondwanaland. *Annual Review of Earth Planetary Sciences* 22, 319–351.
- Stern, R.J., 2002. Crustal evolution in the East African Orogen: a neodymium isotopic perspective. *Journal of African Earth Sciences* 34, 109–117.
- Stern, R.J., Hedge, C.E., 1985. Geochronologic and isotopic constraints on Late Precambrian crustal evolution in the Eastern Desert of Egypt. *American Journal of Sciences* 285, 97–127.
- Stern, R.J., Voegeli, D.F., 1987. Geochemistry, geochronology, and petrogenesis of a Late Precambrian (=590 Ma) composite dike from the North Eastern Desert of Egypt. *Geologische Rundschau* 76, 325–341.
- Stern, R.J., Abdelsalam, M.G., 1998. Formation of continental crust in the Arabian–Nubian Shield: evidence from granitic rocks of the Nakasib suture, NE Sudan. *Geologische Rundschau* 87, 150–260.
- Stern, R.J., Kröner, A., 1993. Geochronologic and isotopic constraints on Late Precambrian crustal evolution in NE Sudan. *Journal of Geology* 101, 555–574.
- Stern, R.J., Voegeli, D., 1995. Late Neoproterozoic (570 Ma) composite dykes from the Northern Arabian–Nubian Shield: Petrogenetic perspectives on contemporaneous mafic and felsic igneous activity. *Third International Dyke Conference, Jerusalem*, p. 69.
- Stoeser, D.B., 1985. Distribution and tectonic setting of plutonic rocks of the Arabian Shield. *Journal of African Earth Sciences* 4, 21–46.
- Stoeser, D.B., Camp, V.E., 1985. Pan-African microplate accretion of Arabian shield. *Geological Society of America Bulletin* 96, 817–826.
- Stoeser, D.W., Frost, C.D., 2006. Nd, Pb, Sr and O isotope characterization of Saudi Arabian Shield terranes. *Chemical Geology* 226, 163–188.
- Streckeisen, A., Le Maitre, R.W., 1979. A chemical approach to the Modal (QAPF) classification of the igneous rocks. *Neues Jahrbuch Mineralogie* 136 (2), 169–206.
- Sun, S., McDonough, W.F., 1989. Chemical and isotopic systematics of oceanic basalts: implications for mantle compositions and processes. *Magmatism in the Ocean Basins*: In: Saunders, A.D., Norry, M.J. (Eds.), *Geological Society Special Publications*, vol. 42, pp. 313–345. London.
- Sylvester, P.J., 1989. Post-collisional alkaline granites. *Journal of Geology* 97, 261–281.
- Tsygankov, A.A., Matukov, D.I., Berezhnaya, N.G., Larionov, A.N., 2007. Late Paleozoic granitoids of Western Transbaikalia: magma sources and stages of formation. *Russian Geology and Geophysics* 48, 156–180.
- Valley, J.W., 2003. Oxygen isotopes in zircon. In: Hanchar, J.M., Hoskin, P. (Eds.), *Zircon: MSA Reviews in Mineralogy and Geochemistry*, vol. 53, pp. 343–385.
- Valley, J.W., Kinny, P.D., Schulze, D.J., Spicuzza, M.J., 1998. Zircon megacrysts from kimberlite: oxygen isotope variability among mantle melts. *Contributions to Mineralogy and Petrology* 133, 1–11.
- Whalen, J.B., Currie, K.L., Chappell, B.W., 1987. A-type granites: geochemical characteristics, discrimination and petrogenesis. *Contributions to Mineralogy and Petrology* 95, 407–419.
- Whalen, J.B., McNicoll, V.J., van Staal, C.R., Lissenberg, C.J., Longstaffe, F.J., Genner, G.A., van Breeman, O., 2006. Spatial, temporal and geochemical characteristics of Silurian collision-zone magmatism, Newfoundland Appalachians: an example of a rapidly evolving magmatic system related to slab break-off. *Lithos* 89, 377–404.
- Yang, J.H., Chung, S.L., Wilde, S.A., Wu, F.Y., Chu, M.F., Lo, C.H., Fan, H.R., 2005. Petrogenesis of post-orogenic syenites in the Sulu Orogenic Belt, East China: geochronological, geochemical and Nd–Sr isotopic evidence. *Chemical Geology* 214, 99–125.
- Yarmolyuk, V.V., Kovalenko, V.I., Kotov, A.B., Salmnikova, E.B., 1997. The Angara–Vitim Batholith: on the problem of batholiths formation in the Central Asia Fold Belt. *Geotectonics* 5, 18–32.
- Yarmolyuk, V.V., Kovalenko, V.I., Salmnikova, E.B., Budnikov, S.V., Kovach, V.P., Kotov, A.B., Ponomarchuk, V.A., 2002. Tectono-magmatic zoning, magma sources, and geodynamic of the Early Mesozoic Mongolo–Transbaikalian magmatic area. *Geotectonics* 36 (4), 293–311.
- Zhao, X.-F., Zhou, M.L., Li, J.-W., Wu, F.-Y., 2008. Association of Neoproterozoic A-type and I-type granites in South China: implications for generation of A-type granites in a subduction-related environment. *Chemical Geology* 257, 1–15.
- Zindler, A., Hart, S., 1986. Chemical geodynamics. *Annual Review of Earth Planetary Sciences* 14, 493–571.